NTNU – Trondheim
Norwegian University of
Science and Technology

Modeling surface nanobubbles in water electrolysis

Asbjørn Hopland Sperre

Master of Science in Physics and Mathematics
Submission date: Januar 2015
Supervisor: Peter Berg, IFY

Norwegian University of Science and Technology
Department of Physics

Abstract

In this project a steady state approach is used to study the stability of surface nanobubbles in water electrolysis. A two dimensional domain is considered, where an electrode of length 100 nm is partly covered by a bubble. The results indicates that a single nanobubble which partially covers the electrode can be stable, as long as the electrogeneration of hydrogen is sufficient to balance the dissolution of hydrogen at near the cap of the bubble. The effect of the evaporation rate constant on the stability of the bubble is investigated, and the results indicates that as evaporation rate constant is increased from 0.01 m/s to a 100 m/s the needed production of hydrogen for a given bubble to be stable decreases. For values outside this range the needed production of hydrogen in converges to a constant value depending on the geometry of the bubble.

Sammendrag

I dette prosjektet benyttes en steady state tilnærming for å studere stabiliteten til en overflate nanobobler i vann-elektrolyse. Et to dimensionalt domene blir studert, hvor en elektrode av lengde 100nm er delvis dekket av av en boble. Resultatene indikerer at en enkel nanoboble som delvis dekker elektroden kan være stabil, så fremt produksjonen av hydrogen er tilstrekkelig stor. Effekten av fordampningsrate konstanten har på stabiliteten til en boble er undersøkt, og resultatene indikerer at når fordamningsrate konstanten øker fra 0.01 m/s til 100 m/s vil den trengte produksjonen for at en gitt boble skal være stabil avta. For verdier utenfor dette intervallet vil den trengte produksjonen av hyrogen konvergere mot en gitt verdi avhengig av geometrien til boblen.

Contents

Values and parameters

Value	Definition	Typical Value
a	Radii of surface coverage	50 nm
C_b	Concentration inside a nanobubble	400 mol/m^3
C_L	Hydrogen saturation concentration	0.8 mol/m^3[6]
D	Hydrogen diffusion-constant in water	$7.5 \cdot 10^{-9}$ m^2/s[6]
H	Henry's constant for hydrogen-water	$1.9 \cdot 10^{-2}$[6]
h	Bubble height	10 nm
j_0	Hydrogen production influx	1 mol/(s·m^2)
p_f	Liquid pressure	10^5 Pa
R	Radii of curvature	0.1μm
R_g	Gas constant	8.314 J/(mol·K)
T	Temperature	298 K
α	Evaporation rate constant	0.1 m/s
γ	Hydrogen-water surface tension	0.07 Pa·m[6]
Δx, Δy	Grid resolution	10 nm
θ	Contact angle	10°

1 Introduction

Nanobubbles are a a nanoscopic phenomenon that has recently been discovered in various areas of interfacial physics, one of them being electrolysis. They should according to classical diffusion theory rapidly dissolve. But many experiments have demonstrated that they are stable, and there has not yet been established a full understanding of their longevity [6] [13] [18] [10]. In electrolysis the high gas concentration seems to be a important factor, both for the formation and as an explanation for their stability.

Electrolysis and fuel cells are a important areas of study, especially for the generation of hydrogen as a renewable energy source. Hydrogen can be used as an efficient energy carrier for fuel cells, which can replace almost all application where fossil fuels are being used today. PEM fuels cells are virtually without any harmful emissions, and the only bi-product is pure water. There exist and are currently being developed many different methods for producing hydrogen, but the most reliable and practical method that are in use today is through water electrolysis. Other studies indicates that there is a potential to produce cheap hydrogen in solar rich areas using PV power plants, and transport the hydrogen to where the power is needed. But for this to be profitable the cost of hydrogen production must be reduced[2]

One of the problems with the hydrogen production in electrolysis, is that the high concentration of hydrogen leads the formation of nanobubbles. These bubble covers the electrode where the gas is being produced, and therefore greatly reduce production efficiency. And as the physics behind the existence and stability of bubbles are not yet fully understood, they constitute an important problem in the production of hydrogen. The subject is quite new, but in recent years many studies, both theoretical and experimental, have been initiated.

1.1 Nanobubbles and longevity

In experiments there are observed three different types of nanobubbles, bulk-, surface nanobubbles and micropancakes. Bulk bubbles are spherical bubbles suspended in bulk liquids, with a typical radii of 50-100 nm. Surface nanobubbles are spherical caps found at the solid/liquid interface, with a typical radii of curvature of 100-1000 nm and heights and width of 5-20 and 50-100 nm, respectively. Micropancakes are also found at the solid/liquid interface and is observed with widths of order of several hundred nanometer, with a height of just 1-2 nm [13]. There is not completely understood whether or not there is a link between surface bubbles and micropancakes.

1.2 Electrolysis

Electrolysis is a well known technique to drive a non-spontaneous chemical reaction using a direct current, such a chemical reaction can be the separation of water to hydrogen and oxygen,

$$2H_2O \rightleftharpoons O_2 + 4H^+ + 4e^-.$$
$$2H_2O \rightleftharpoons O_2 + 2H_2$$

Another application of such a chemical reaction can be to run the process in reverse by instead of *applying* energy trough a current, such as the case in the electrolysis, one can *receive* energy through a current by applying the gases (e.g. oxygen from the air and stored hydrogen). Such a device, that convert chemical energy to electric energy, is called a fuel cell.

The most common method used in electrolysis is the Polymer electrolyte membrane (PEM) electrolysis, where one separate the cathode and anode with a polymer membrane. The reduction of water is occurring at the anode, and the protons can move trough the membrane, where as the oxygen or hydrogen will have a small cross-over rate. The reduction of the protons then occur at the cathode, and the power source drives the electrons from the anode to the cathode. At each electrode there will occur a production of gas, and if the gas concentration becomes high enough the formation of nanobubbles can occur.

1.3 Hydrogen nanobubbles in water electrolysis

The observed nanobubbles are very flat, and have radii of order, $a \approx 50$nm at the surface and a height $h \approx 10$nm, which yields a low contact angle of $\theta \approx 10^\circ$ [3]. Classical theory of diffusion yields that such small bubbles should dissolve on a time scale of microseconds, but in experiments they seem to last for several hours ($\mathcal{O}(10^4)$ seconds), or even days [18].

1.4 Latest work

Many experiments have observed the longevity of nanobubbles, and formed both in clusters and on a single nano electrode. By varying the applied voltage or the reaction time the formation and growth of bubbles can be precisely controlled.[18] [17] [5]. The numerical work on nanobubbles is mostly done by using molecular dynamics, which can quickly become cumbersome. Other works, such as Brenner and Lohse [13], have demonstrated that a near wall gas enrichment can be used to explain a dynamic equilibrium.

1.5 Thesis outline

The scope of this thesis is to examine the scaling of the lifetime of surface nanobubbles through a simple model using a finite difference scheme, with a specific interest for the evaporation rate constant, α, and its impact on the longevity of a nanobubble. Using a diffusion flow hydrogen through the liquid phase and Henry's Law to model the rate of flow between the gaseous- and liquid phase, a simple model for a half-cell reaction is obtained.

A quadratic domain of 500×500 nm is considered, with a electrode of a 100 nm partially covered by a bubble. The domain is discretized by dividing it into a uniform grid. A Dirichlet boundary condition is imposed on the sides far away from the electrode, and a Neumann boundary condition is imposed on the two other sides of the domain, except for at the electrode. A bubble of a certain geometry is imposed on the system, partially covering the electrode and therefore reducing the net production of hydrogen. The production of hydrogen at the free area of the electrode is imposed on the system as a Neumann boundary condition.

First a simple model of a completely flat bubble with a Neumann boundary condition of zero flux is imposed on the system. The solution of the steady state diffusion equation is then computed for the system, in order to obtain the concentration profile of the system. The total system cannot be claimed to be a steady state solution as long as there is not a nonzero flux between the phases, as this would imply a change of size of the bubble. The net flux between the phases is dependent on the contact angle, and the calculated concentration profile is not. Therefore the contact angle that yields a zero net flux can be calculated for the imposed conditions on the system.

A second model is then considered, where the geometry of the bubble is included in the model. A Robin boundary condition is imposed on the system along the surface of the bubble, as the flux between the phases will depend on the concentration in the liquid. The concentration profile for the system can then be calculated by solving the steady state diffusion equation for the model. As in the flat bubble approximation, the system cannot be claimed to be a steady state solution as long as there is a nonzero flux between the phases. The imposed flux at the electrode must then be varied in order to obtain a concentration profile that yields a zero net flux between the phases.

2 Experimental evidence

2.1 Experiments and numerical work

An important paper for this thesis is the experiment conducted by Lou and White[6], where an single nanobubble is formed on an electrode of length 50 nm. The observation is that there is a sudden drop in the current associated with the transport-limited reduction of protons, the decrease in current is in equivalent with a $\sim 95\%$ blockage of the electrode. Other experiments have observed and controlled the growth of the bubbles by varying the applied current.[17]. The process is recorded with AFM measurements, and the observed effect is that the bubble grows until it reaches a dynamic equilibrium.

At larger electrodes the bubble clusters are formed [18], where the formation, growth and coalescence of bubbles are recorded using in-situ tapping mode atomic force microscopy, an example of such images is shown in figure 1

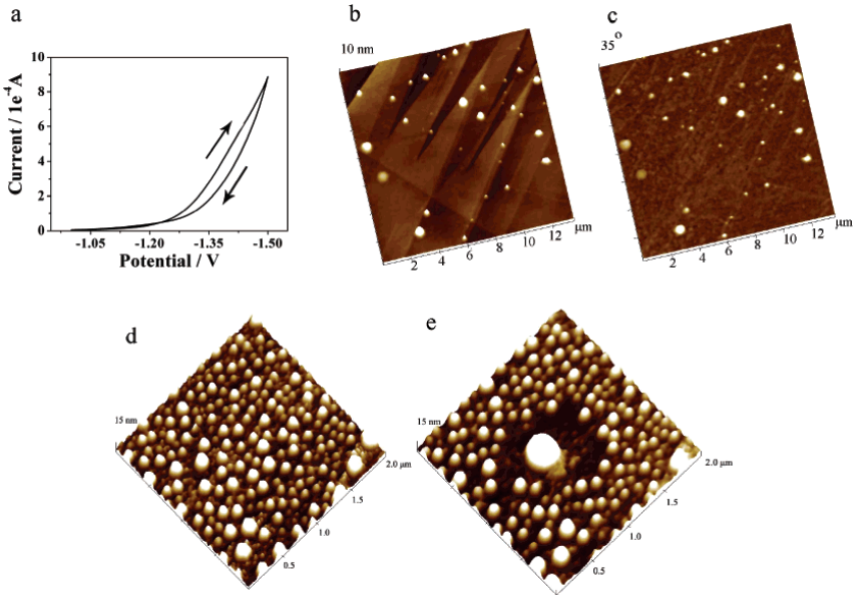

Figure 1: Electrochemically generated nanobubbles on a highly oriented pyrolytic graphite surface. (a) CV curve recorded at a scan rate of 0.2 V/s. (b) Height and (c) phase images of of generated nanobubbles (light spherical cap features) after a voltage of -1,5 V being applied for 10s. TMAFM images of nanobubbles obtained after applying a voltage of -2.1 V for 2 s (d) before and (e) after tip pertubation. [18, figure 1]

The spatial distribution of surface nanobubbles in such clusters is found not to be randomly distributed lhuissier2014spatial, which is attributed to the history of nucleation during the formation of the bubble. The sizes a nanobubble in such a cluster is found to be strongly correlated with the area of the bubble-depleted zone around it. This correlation indicates that the bubble growth is due to diffusion of gash through the liquid and through gas absorbed on the surface. This effect is shown in figures 2 and 3.

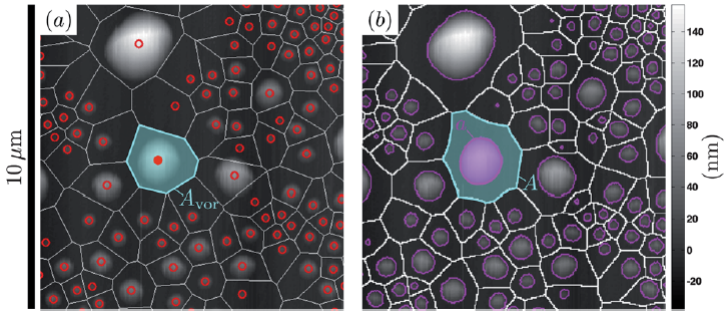

Figure 2: Portion of a typical AFM image of nanobubbles. (a) The cellular diagrams depicted is Voronoi diagrams constructed from the bubbles center (red circle). (b) Modified Voronoi diagram based on the bubbles triple contact line (pink line). The bubbles footprint (colored pink), is associated with the modified Voronoi cell (cyan). The bubble footprint has an area a, and the area of the modified Voronoi diagram has an area A [5, figure 1]

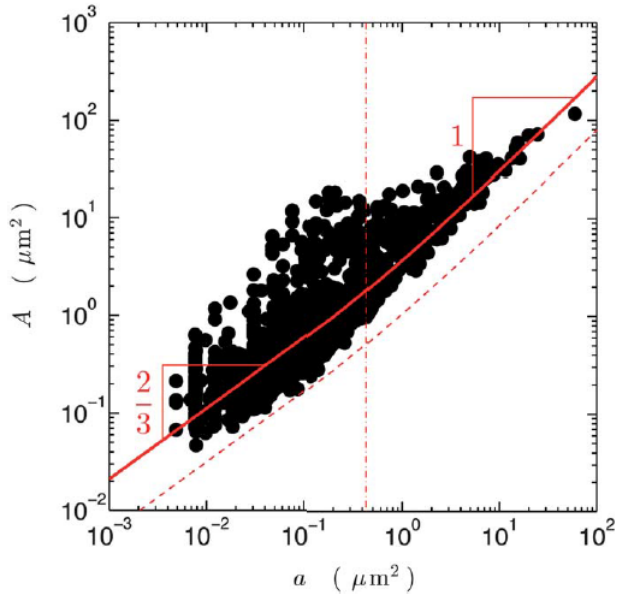

Figure 3: The area A of the modified Voronoi cell plottet versus the area a from figure 2, where the correlation between the modified Voronoi cell of a bubble and its radii is shown. [5, figure 4]

Most of the numerical work regarding nanobubbles are models using molecular dynamics. It is very very cumbersome, but can be effective in determining macroscopic thermodynamic properties for systems that obey the ergodic hypothesis [7] [12].

2.2 Dynamical equilibrium

Bubbles with radices in the scale of 100nm-1μm would by classical diffusion theory dissolve at a timescale of microseconds.[11] But the observed lifetime of the bubbles are at least 10-11 orders of magnitude longer, so they are quite stable. There are two popular explications for this longevity of the bubbles, contamination and a dynamic equilibrium.

The contamination explanation is that the presence of insoluble contaminates (e.g. polymers) accumulate on the liquid/gas interface, the surface tension will decrease and a barrier preventing diffusion will be formed. The lowering of the surface tension will cause the driving force of the dissolution to be greatly reduced. If the contaminants become pinned to the bubble, the density of the contamination will increase as the bubble shrinks. This will in turn lead to a further decrease in surface tension. As the pressure difference (Laplace pressure), is proportional to the surface tension, this will also decrease. One can even achieve a negative surface tension. Then the only driving force for the dissolution of the bubble will be the increase in entropy by mixing of components, which often will take an incredible long time. The problem with this explanation is the assumption of the presence of containments, the formation of nanobubbles are found in many different systems with different techniques and chemicals. Even the most purified chemical solutions will contain contaminants, if not extraordinary measures are taken. And the small surface of the bubble will then yield that the need for contaminants to cover the surface of the bubble is equally small. A more problematic side of the explanation is the contamination will only decrease the diffusive outflux, and not completely prevent it. This is due to the fact of thermal fluctuations of the contaminate layer, which will the imply that there will always be "holes" in the contaminate layer. Therefore there will always be an diffusive outflux present, possibly greatly reduced, albeit always present. One would then expect to observe a slow reduction in size over time, but nanobubbles are shown to have a stable volume in experiments.

A more accepted theory is the dynamic equilibrium model, which uses near-wall gas enrichment as a replenishing gas source. The theory is that gas concentration will be higher near the hydrophobic wall, and therefore there can be an influx of gas near the wall and as the concentration decreases as one approaches the top of the spherical cap, there will be an outflux. Then as long as the bubble is small enough, there will be an total influx, which will lead to a increased volume. Or if the bubble is larger than a critical value there will be a net outflux, and the volume will decrease. Then there should be a critical size when the influx near the wall will balance the outflux at the top. This could explain the stability of nanobubbles, and the preferred sizes observed experimentally.

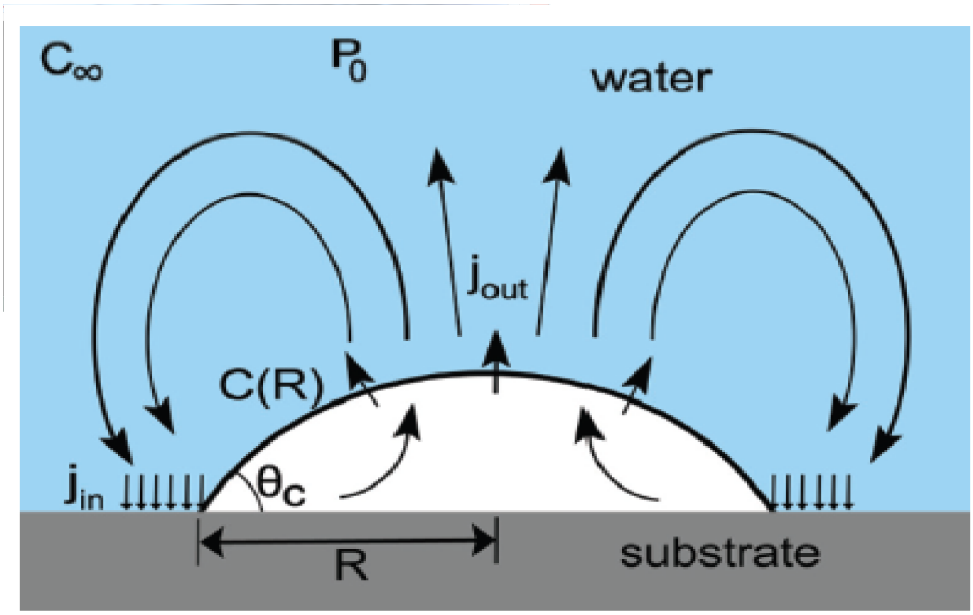

Figure 4: Dynamic equilibrium model using near wall gas enrichment. Near a hydrophobic substrate the concentration of dissolved gas is higher than at the top, and this could lead to a net flux of zero here the outflux at the to, j_{out}, cancels the influx near the substrate, j_{in}.[figure 1 (a)] [10]

There are however some aspects with the dynamic equilibrium that needs to be explained, if the net influx at the wall is to be upheld while a net outflux occurs at the top of the bubble. There needs to be a replenishing of the gas that flows from the fluid in to the bubble, and out from the top. As shown in figure 4, there would also be a need for an energy source that drives the flow of gas.

In a half-cell reaction with a formed bubble, there will obviously be a replenishing of the gas near the surface form the half-cell reaction and a the energy source is the applied current. Such dynamically stabilized nanobubbles are observed in experiments, where a surface nanobubble partly covers the electrode [6].

3 Modelling

3.1 General theory

3.1.1 Diffusion

Diffusion is a term used to describe the spontaneous movement of a substance, and at a macroscopic scale is recognized as the net movement of a substance from regions with high concentration to regions with low concentration. Diffusion can often be described through a flux, $\vec{J}$, that is proportional to a concentration gradient, ∇C. This relation is known as Fick's first law,

$$\vec{J} = -D\nabla C, \tag{1}$$

where the proportionality constant, D, is called the diffusion constant. This relation is only valid at a steady state. To describe the concentration profile over time one has Fick's second law, which can be derived from mass-conservation and Fick's first law. By considering a small control volume one can show that,

$$\frac{\partial C}{\partial t} = -\nabla \cdot \vec{J}, \tag{2}$$

by applying the applying the divergence operator Fick's first law, and using [2] one get;

$$\nabla \cdot \vec{J} = -\nabla \cdot (D\nabla C), \tag{3}$$

$$\frac{\partial C}{\partial t} = D\nabla^2 C, \tag{4}$$

assuming D is constant in space.

3.1.2 Laplace pressure

The pressure difference between the inside and outside of a curved surface is known as the Laplace pressure, which can be determined from the Young-Laplace equation,

$$\Delta p = p_{in} - p_{out} = \gamma \left(\frac{1}{R_1} + \frac{1}{R_2} \right). \tag{5}$$

Where the R denotes the radii of curvature and γ is the surface tension between the fluid and liquid. If the curved surface is a sphere, or a segment of a sphere, the principal radii of curvature are identical.

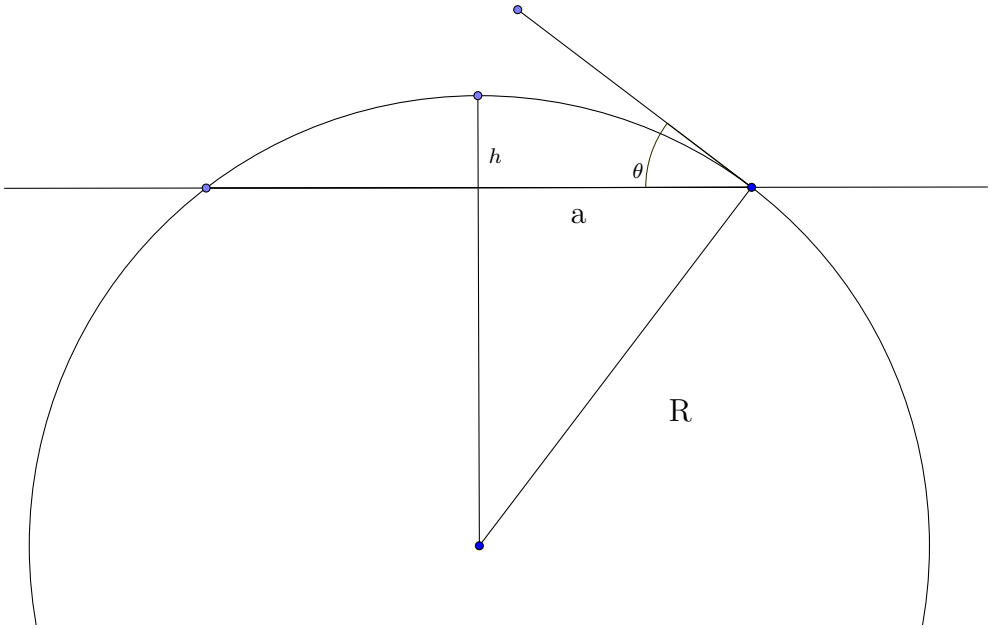

Figure 5: Geometry of a surface nanobubble, with radii of curvature R, contact angle θ, height h and surface coverage radii a.

It is often more useful in such cases as in figure 5 to use the contact angle between the liquid and gaseous phase, and the radii of the bubble. Through trigonometry it is trivial to deduce that the pressure-difference can be expressed as,

$$\Delta p = \frac{2\gamma}{R} = \frac{2\gamma \sin(\theta)}{a}. \tag{6}$$

If the ideal gas law is assumed to hold for the gas in the bubble, the concentration inside the bubble can be expressed as,

$$C_b = \frac{n}{V} = \frac{p}{R_g T} = \frac{1}{RT}\left(p_f + \frac{2\gamma \sin(\theta)}{a}\right), \tag{7}$$

where p_f is the pressure in the fluid.

3.1.3 Henry's Law

Henry's law states that of a given temperature and volume the amount of dissolved gas in a liquid is directly proportional to the partial pressure of the gas in equilibrium with that liquid. That is,

$$p_{partial} = H_p C^*_{aq}, \tag{8}$$

where $p_{partial}$ is the partial pressure of the gas in the solute and C^*_{aq} is the concentration of the solute. H_p is refereed to as Henry's constant, and could also be defined as a

dimensionless quantity at a given temperature and pressure. The dimensionless Henry's constant, H, is then defined as,

$$H = \frac{C^*_{aq}}{C^*_{gas}}. \tag{9}$$

A common mathematical model for describing the net flux per unit area, across a surface is to assume it is proportional to the concentration difference from the equilibrium

$$J = \alpha(C_{aq} - HC_{gas}). \tag{10}$$

Here the flux is defined as positive from the aqueous solution to the bubble. One can explain the motivation for equation [10] from the mathematical modelling principle that it is the simplest form of describing the flux whilst upholding that the flux at equilibrium is zero and the increase or decrease in either concentration will lead to, respectively, an increased or decreased flux in the opposite direction. A Taylor expansion around the equilibrium C^*_{aq}, C^*_{gas}, can further support the reasoning behind the model, assuming the flux only depend on the respective concentrations.

$$J(C_{aq}, C_{gas}) = J(C^*_{aq}, C^*_{gas}) + \left.\frac{\partial J}{\partial C_{aq}}\right|_{eq} (C_{aq} - C^*_{aq}) + \left.\frac{\partial J}{\partial C_{gas}}\right|_{eq} (C_{gas} - C^*_{gas}) + \mathcal{O}(2). \tag{11}$$

Where the fist term, the flux at equilibrium, is obviously zero. The easiest approach to treat the expression, is to expand the flux around a point where one of the concentrations is held at equilibrium. This is due to the fact that there is infinitely many equilibrium concentrations, and there is no trivial way to proceed. However, in a steady state system, with a bubble of constant size and concentration will be the equilibrium concentration, and therefore $C^*_{gas} = C_b$, where C_b is the concentration of gas in the bubble. By inserting equation [9] into equation [11], an approximation for J is obtained,

$$J \approx \left.\frac{\partial J}{\partial C_{aq}}\right|_{eq} (C_{aq} - HC_b) \tag{12}$$

$$= \alpha(C_{aq} - HC_b). \tag{13}$$

This is equivalent to calculating the Taylor series and approximating the infinitesimally increased concentration with the use of Henry's law, $C^*_{aq} \approx HC_g = H(C^*_g + \Delta C_g)$ and vice versa. As Henry's law reflects the relative concentrations at equilibrium, the expression can not be claimed to be a proof for equation 10. However the linear dependence is proven in the expansions where one of the concentrations is held at equilibrium, yields an approximation that is second order accurate assuming Henry's Law holds.

3.2 Finite difference and one-sided derivatives

The finite-difference method uses a grid and a combination of discrete function values at the grid points to numerically solve a set of PDEs. The partial derivative at a grid point

can be approximated through the function values at neighbouring points and the finite difference between the grid points. There are three different types of finite differences, central difference (second order accurate), forward- and backwards difference (first order accurate). Finite difference techniques work fine for all interior points of a domain, where all the neighbouring points lie inside of the domain. The boundary will by definition have some neighbouring points that lie outside of the domain, and only forward- or backwards differences can be defined through grid points inside of the domain and next to the boundary. It is therefore impossible to express higher orders of partial derivatives at the boundary, and an approximation of functions partial derivative will only be first order accurate. Any boundary condition that specifies the values of the functions derivatives, or some combination of different orders of derivatives, will therefore need other methods of approximations to uphold second order of accuracy.

A way to achieve a higher order of accuracy is to calculate the derivatives at the boundary as one-sided derivatives. The method can be derived through a Taylor expansion of the function to obtain an expression for the derivative.

$$u(x) = u(0) + x\left(\frac{\partial u}{\partial x}\right)_{x=0} + \frac{x^2}{2}\left(\frac{\partial^2 u}{\partial x^2}\right)_{x=0} + ... \tag{14}$$

$$\approx a + bx + cx^2 \tag{15}$$

$$\frac{\partial u}{\partial x} \approx b + 2cx, \tag{16}$$

$$\left(\frac{\partial u}{\partial x}\right)_{x=0} \approx b. \tag{17}$$

The function value at a distance, x, is approximated up to the second order of the distance, and the derivative evaluated at the boundary is expressed as some constant, b and c for the second and third order respectively. Now by setting the distance between the points to Δx, and inserting into the expression for u, one obtains,

$$u_0 = a, \tag{18}$$

$$u_1 = a + b(\Delta x) + c(\Delta x)^2, \tag{19}$$

$$u_2 = a + 2b(\Delta x) + 4c(\Delta x)^2. \tag{20}$$

There are three equations, with three unknowns, a, b and c, so it is straightforward to solve the set of equations, for the first-order derivative at the boundary:

$$b = \left(\frac{\partial u}{\partial x}\right)_0 = \frac{-3u_0 + 4u_1 - u_2}{2\Delta x}. \tag{21}$$

The error can be analysed, by inserting the derived expression into the Taylor expansion for the function.

$$\left(\frac{\partial u}{\partial x}\right)_i \approx \frac{\alpha u_i + \beta u_{i+1} + \gamma u_{i+2}}{\Delta x} \tag{22}$$

$$u_{i+1} = u_i + \Delta x \left(\frac{\partial u}{\partial x}\right)_i + \frac{(\Delta x)^2}{2}\left(\frac{\partial^2 u}{\partial x^2}\right)_i + \frac{(\Delta x)^3}{3!}\left(\frac{\partial^3 u}{\partial x^3}\right)_i + ... \tag{23}$$

$$u_{i+2} = u_i + 2\Delta x \left(\frac{\partial u}{\partial x}\right)_i + \frac{(2\Delta x)^2}{2}\left(\frac{\partial^2 u}{\partial x^2}\right)_i + \frac{(2\Delta x)^3}{3!}\left(\frac{\partial^3 u}{\partial x^3}\right)_i + ... \tag{24}$$

By using these expressions for the two nearest neighbours of the boundary point, and expressing the approximation for the first order derivative in terms of the Taylor expansion, one obtains

$$\left(\frac{\partial u}{\partial x}\right)_i \approx \frac{\alpha u_i + \beta u_{i+1} + \gamma u_{i+2}}{\Delta x} \tag{25}$$

$$= \frac{\alpha + \beta + \gamma}{\Delta x} u_i + (\beta + 2\gamma)\left(\frac{\partial u}{\partial x}\right)_i + \frac{\Delta x}{2}(\beta + 4\gamma) + \mathcal{O}(\Delta x^2.) \tag{26}$$

$$\tag{27}$$

For the approximation to be second-order accurate one has to have the left hand side (the expression that was previously derived as equation [21)], to be equal to the first-order derivative plus the higher order terms. One then obtains

$$\alpha + \beta + \gamma = 0, \quad \beta + 2\gamma = 1, \quad \beta + 4\gamma = 0. \tag{28}$$

$$\Rightarrow \gamma = -1/2, \quad \beta = 2, \quad \alpha = -3/2. \tag{29}$$

$$\Rightarrow \left(\frac{\partial u}{\partial x}\right)_0 = \frac{-3u_0 + 4u_1 - u_2}{2\Delta x} + \mathcal{O}(\Delta x^2). \tag{30}$$

This then proofs that equation [21] is second order accurate.

3.3 Model domain

A two dimensional representation cathode half cell of a water electrolysis with a nanobubble centred is illustrated in figure 6.

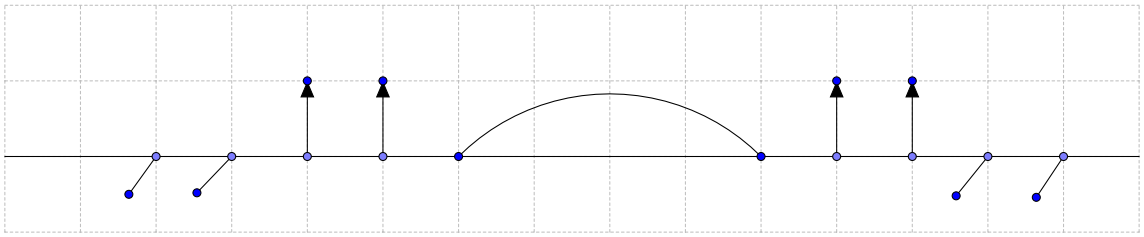

Figure 6: Illustration of the half cell, arrows indicate a flux.

The hydrogen is generated on a electrode, e.g patina, which is partly covered by a nanobubble in the center of the electrode. There is trivial to see that due to the symmetry

of the half cell that the problem can be solved by inspecting the left or right half of the half cell and using a no flux condition where the split the cell. Further there is assumed to be a constant hydrogen generation per unit area, j_0, and that the rest of the bottom of the cell is a solid which yield a no flux condition. And far away from the electrode the hydrogen concentration is at saturation level, C_L. To use a finite difference scheme to solve the steady state problem, a grid has to be defined to express the derivatives, illustrated in figure 7.

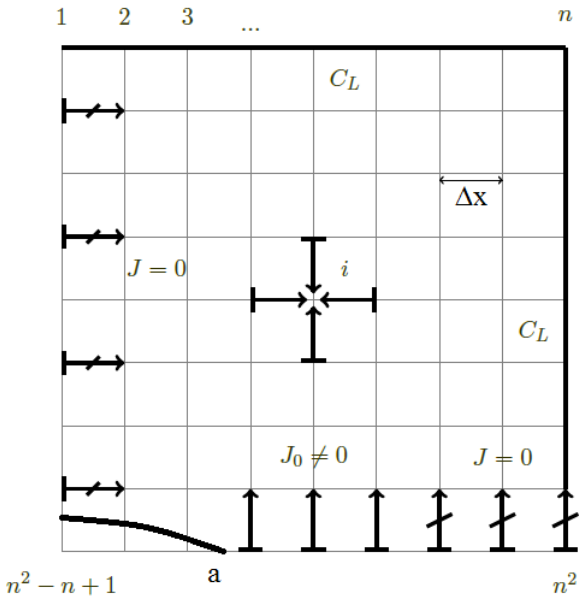

Figure 7: Representation of model system, which is divided into $(n-1)\times(n-1)$ domains. The electrode is located in the bottom left corner, partially covered by the bubble with radii a. The flux at the electrode is set to j_0, and along the rest of the bottom and the left side of the domain there is imposed a no flux condition. At the top and right side of the domain the concentration is set to the saturation condition, C_L. The grid points are labelled from 1 in the top left corner to n^2 in the bottom right corner.

If the grid-points is labelled from 1 to n^2, her from top left to right, top to bottom. If one uses a finite differences scheme to set up an equation for each point, one obtains a set of n^2 equations with as many unknowns. And one can write the set of equations as,

$$\mathbf{A}\vec{C} = \vec{b}. \tag{31}$$

Here $\vec{C}$ is the column vector of length n^2, containing the concentration at all of the points - which is what one wants to find. And the $n^2 \times n^2$ matrix, $\mathbf{A}$ is the indices matrix, reflecting the dependence between the concentrations, and $\vec{b}$ is the boundary values is stored in a column vector.

3.3.1 Interior points

To set up the equations for the interior points, Fick's second law is applied, and assuming no mass accumulation there is easy to show that the equation for a point i is:

$$D\frac{C_{i+1} + C_{i-1} + C_{i+n} + C_{i-n} - 4C_i}{\Delta x^2} = 0. \tag{32}$$

Then these equations can be represented in the matrix equation, one for each interior point and each of them corresponds to a row in the matrix equation, j,

$$A_{j,i} = -4 \tag{33}$$
$$A_{j,i-1} = A_{j,i+1} = A_{j,i-n} = A_{j,i+n} = 1. \tag{34}$$
$$b_j = 0 \tag{35}$$
$$\tag{36}$$

3.3.2 Saturation boundary condition

For all of the boundary points at saturation level for the involved gas, the equations are quite straightforward

$$C_i = C_L \tag{37}$$
$$\tag{38}$$

When converted to matrix form, the equation for the relevant points becomes

$$A_{j,i} = 1, \tag{39}$$
$$b_j = C_L. \tag{40}$$

3.3.3 Flux boundary condition

Along the other boundaries one has a flux boundary condition, and these can be implemented by using Fick's first law and applying the one sided derivative. It clearly seen that the equation for the no flux boundary condition to in the left side of the domain becomes

$$D\frac{-3C_i + 4C_{i+1} - C_{i+2}}{2\Delta x} = 0. \tag{41}$$
$$\tag{42}$$

The no flux boundary condition along the bottom of the domain, will be similar to the left side,

$$D\frac{-3C_i + 4C_{i-n} - C_{i-2n}}{2\Delta x} = 0. \tag{43}$$
$$\tag{44}$$

Implemented in the matrix equation, equation for the relevant points becomes

$$A_{j,i} = -3 \quad A_{j,i+1} = 4, \quad A_{j,i+2} = -1 \text{ For the left side} \tag{45}$$
$$A_{j,i} = -3 \quad A_{j,i-n} = 4, \quad A_{j,i-2n} = -1 \text{ For the bottom.} \tag{46}$$
$$b_j = 0. \tag{47}$$

Assuming that the gas production occurs at a constant rate, wit a net flux of j_0, perpendicular to the surface, one will similarly as the no-flux boundary condition use the one sided derivative, with another boundary value

$$-D\frac{-3C_i + 4C_{i-n} - C_{i-2n}}{2\Delta x} = j_0. \tag{48}$$
$$\tag{49}$$

Implemented in the matrix equation, equation for the relevant points becomes

$$A_{j,i} = -3 \quad A_{j,i-n} = 4, \quad A_{j,i-2n} = -1 \tag{50}$$
$$b_j = -\frac{2j_0\Delta x}{D}. \tag{51}$$

3.4 Flat bubble approximation

To be able to complete the boundaries, one has to impose a boundary condition at the liquid-vapour interface. To include the curvature of the bubble, the gas occupy a certain volume above the disk. The simplest approach is to use the fact that the measured contact angles for nanobubbles is very low, and use this legitimize an approximation of a flat bubble. And by assuming steady state and, still be able calculate the concentration distribution. One would the further also assume a no flux boundary at the gas-liquid interface. And therefore the boundary condition at the bubble is the same as the no flux boundary condition.

It is now easy to us a two step approach to investigate whether or not a stable surface bubble can exist under the imposed conditions. By using 10 with the bubble concentration calculated from equation [7], the flux of gas between the liquid-gas interface can be calculated. As there is assumed a steady state, the only valid result is that of which will yield a net flux of zero. This is due to the effect that otherwise the bubble will grow or shrink, and the system can not be claimed to be in a steady state.

The procedure is then thus use a numerical integration scheme, and the flux per unit time is integrated over the bubble surface. And using the flat bubble approximation, the integration would be trivial to calculate by applying the trapezoidal rule [1]. Assuming the bubble stretches over m domains of length h, over a distance equal to the length of the surface a. And assuming a uniform distribution of the gas inside the bubble, the integration becomes,

$$J_{tot} = \int_{x_0}^{x_m} J(s)dx = \alpha \sum_{i=0}^{m-1} \int_{x_i}^{x_{i+1}} (C_{aq}(x) - HC_g)dx \tag{52}$$

$$\approx \alpha \left[\frac{h}{2} \sum_{i=0}^{m-1} (C_{aq}(x_i) + C_{aq}(x_{i+1})) - SHC_g \right] \tag{53}$$

$$= \alpha \left(I_b - SHC_g \right). \tag{54}$$

Where J_tot, is the definite integral of the flux over the bubble.

As the contact angle is not needed in order to compute the concentration profile, it can be changed in order to achieve a zero net flux over the surface of the bubble. Thus by solving $J_{tot} = 0$, the contact angle for a steady state system can be calculated to be,

$$\sin(\theta) = \frac{RTI_b - HSp_f}{2H\gamma}. \tag{55}$$

3.5 Including bubble curvature

To include the bubble in the numerical scheme, a problem that arises is illustrated in figure 8

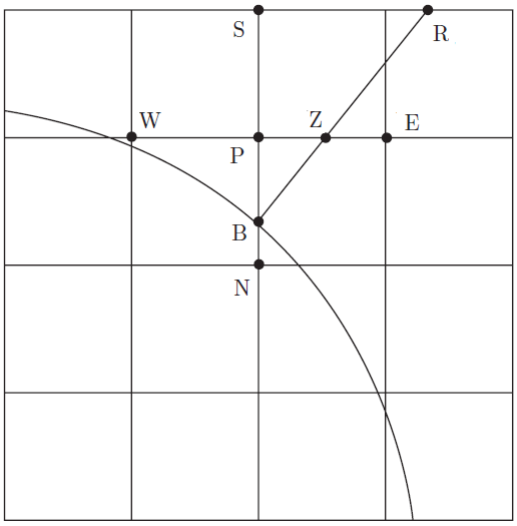

Figure 8: External boundary point

The problem that arises is the occurrence of points like P in figure 8, where one, or more of the neighbouring points are at the boundary. It is obvious that such points cannot be approximated as in [32], when the point N lies on the other side of the boundary, and the point B is closer to point P than S.

An approximation can be obtained by calculating the first partial derivative at the halfway point, P_+, halfway between N and P, and P_- halfway between P and B.[9]

$$\frac{u_N - u_P}{y_N - y_P} = \frac{\partial u}{\partial y}(P_+) \tag{56}$$

$$\frac{u_P - u_B}{y_P - y_B} = \frac{\partial u}{\partial y}(P_-). \tag{57}$$

$$\tag{58}$$

The distance between these two half-way points is $(y_N - y_B)/2$. Further the distance $y_P - y_B = \beta\Delta y$, where Δy is the grid size and $0 < \beta < 1$. Thus the second partial derivative can be expressed as

$$u_{yy} \approx \frac{2}{y_N - y_B}\left(\frac{u_N - u_P}{y_N - y_P} - \frac{u_P - u_B}{y_P - y_B}\right) \tag{59}$$

$$\approx \frac{2u_N}{(\beta+1)(\Delta y)^2} - \frac{2u_P}{\beta(\Delta y)^2} + \frac{2u_B}{\beta(\beta+1)(\Delta y)^2}. \tag{60}$$

The equations for such points will be the same as for other interior point, except for the correction of β, which has to be calculated for each point. To set up the indices matrix for such points is then similar to the other exterior points, but each point will have to be individually treated when the β will in differ for each point. The equation for points such as P, with a correction for the u_{yy}-derivative,

$$A_{j,P} = -2 - \frac{2}{\beta} \tag{61}$$

$$A_{j,W} = A_{j,E} = 1 \tag{62}$$

$$A_{j,B} = \frac{2}{\beta(\beta+1)} \tag{63}$$

$$A_{j,N} = \frac{2}{\beta+1} \tag{64}$$

$$b_j = 0. \tag{65}$$

$$\tag{66}$$

Where $A_{j,P}$ etc. indicate the indices for point P and so forth. The approximation is obviously upheld for both coordinates, and due to the linearity of the laplacian the derivative in each direction is independent of each other. Therefore in cases such as W in figure 8, u_{xx} will have to be approximated in similar fashion. Further such points has to be taken into account when setting up the equations for the interior points. An easy way to do this, is to consider the rectangle that is spanned by the grid lines of the horizontal grid line that is just above the bubble height and the vertical line that is just to the left where the bubble surface intersect the electrode. Points outside of this domain will not have any neighbours that lies inside of the boundary.

Estimating the the derivative in such a manor is equivalent to extrapolating from interior and boundary points to a fictitious exterior point, and then applying the standard difference scheme. A quadratic extrapolation of u_S in figure 8 would yield equation [60].

To still have a well defined problem, a set of equations is needed for the points added along the boundary to the model. It is possible to define a no flux condition as in

the flat bubble approximation, but it is almost as simple to impose a Robin boundary condition along the normal to the surface and applying [10]. Thus the flux, Neumann boundary condition, should depend on the concentration, Dirichlet boundary condition, at the boundary. The normal derivative for these boundary points has to approximated, and can be approximated by investigating figure 9.

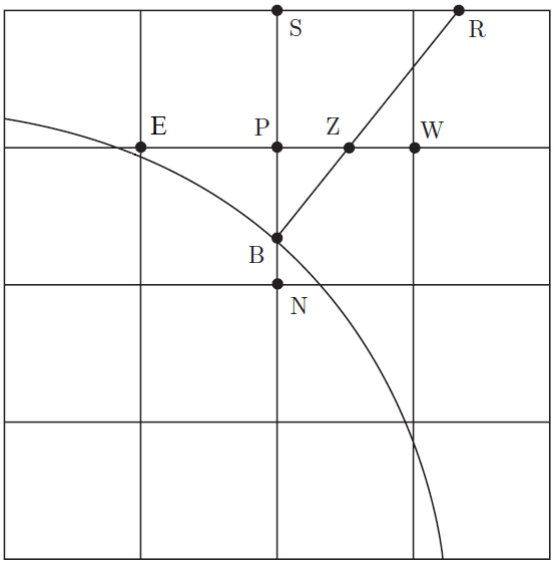

Figure 9: Normal derivative at a curved boundary

A normal derivative can be approximated by assuming that the normal at B meets the horizontal mesh line EPW at Z and suppose the lengths are,

$$ZP = p\Delta x, \quad PB = \beta\Delta y, \quad BZ = q\Delta y, \tag{67}$$

where $0 \leq p \leq 1$, $0 \leq \beta \leq 1$ and $0 < 1 \leq \sqrt{1 + (\Delta x/\Delta y)^2}$. The normal derivative can be approximated by,

$$\frac{\partial u}{\partial n} \approx \frac{u_B - u_Z}{q\Delta y}. \tag{68}$$

An approximation of the value of u_Z can be obtained by linear interpolation between u_W and u_P,

$$u_Z \approx pu_W + (1-p)u_P. \tag{69}$$

Thus the normal derivative can be approximated by,

$$\frac{\partial u}{\partial n} \approx \frac{u_B - pu_W - (1-p)u_P}{q\Delta y}. \tag{70}$$

The flux between the liquid and gaseous phase is govern by equation [10], and by inserting the approximation for the normal derivative, the indices matrix can be obtained.

$$A_{j,W} = p/q \tag{71}$$
$$A_{j,P} = (1-p)/q \tag{72}$$
$$A_{j,B} = -1/q - \Delta y\alpha/D \tag{73}$$
$$b_j = -\alpha\Delta y H C_b/D. \tag{74}$$

In both cases where the points where the bubble and the mesh intersects has to be found for each bubble, when the points will depend on the geometry of the bubble and the resolution of the mesh. Its trivial to solve this geometrical problem through parametrizing the bubble surface as a spherical cap with a given radius and center. The normal at any given point along the surface will obviously be parallel with the straight line from the point to the center.

3.5.1 Steady state solution

A steady state system is a system where all time derivatives are zero, and therefore the model represents a steady state system as long as the net flux between the bubble and liquid is zero. The net flux into the bubble can be calculating by integrating equation [10] along the surface, S, of the bubble.

$$J_{net} = \alpha \int_S (C_{aq} - HC_b) dS. \tag{75}$$

As in the flat bubble approximation, the trapezoidal rule[1] can be applied to evaluate the integral over the surface. If the boundary points at the surface is labelled from 1 to N, with x-values increasing with N, the integral can be approximated as,

$$J_{net} \approx \alpha R \left(\frac{1}{2} \sum_{i=1}^{N-1} \left[(C_i + C_{i+1}) \arcsin\left(\frac{x_{i+1} - x_i}{R} \right) \right] - HC_b\theta \right). \tag{76}$$

Since the distance between the points in genera differ, each surface segment will have to be individually evaluated.

In the flat bubble approximation the contact angle needed not to be to defined to set up the equations, and could therefore be changed in order to achieve a net flux if zero. When the curvature of the bubble is included all parameters has to be set in advance, and it is no longer possible to change any parameters without imposing a change in concentration profile.

To achieve a net flux equal to zero, the most reasonable approach is to vary j_0 for a given geometry. This is of course due to the fact that only a few rows of column vector $\vec{b}$ will change. Further one knows that when no production of hydrogen occur, there will be a net outflux from the bubble. And if a high enough production of hydrogen occurs, then there will be a net influx. Thus a bijection can be used to find an influx j_0 in order to achieve a net flux of zero. The bijection method is well known, and is a product of the intermediate value theorem. By setting the minimal value for the bijection method at 0, and the maximum at a sufficiently large flux, one can iterate until the net outflux is essentially zero.

3.6 Bulk nanobubble dissolution

To show how the α effects the time for a bubble to dissolve, it is easy to compare the results with that of a simple model for a bulk bubble dissolution in three dimensions. Where the same approximations, isothermal and mechanical equilibrium, is still assumed. Further one assumes that the process is slow, namely that the speed of which the surface move is slow.

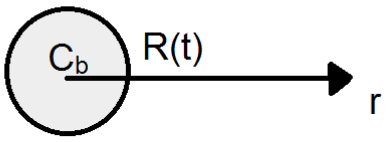

Figure 10: Bulk bubble dissolution for a bubble with concentration C_b, and radii $R(T)$

The equations for the system is trivial to set up, where the concentration inside the bubble can be found from equation [7],

$$C_b = \frac{2\gamma + Rp}{RTR_g}. \tag{77}$$

And the concentration profile in the liquid is calculated from equation [2], with appropriate boundary conditions, the first being that the concentration falls off to zero as r goes to infinity, the other will depend on dissolution of gas from the bubble. To solve the laplacian in three dimensions with isotropy is straightforward, and the concentration in the liquid can be expressed as,

$$C(r) = A/r + B = A/r. \tag{78}$$

To simplify the model, the two extreme cases where α goes to zero and infinity can be considered. When α is close to zero, the flux at the bubble boundary will be determined by a flux balance between the outflux from the bubble - [10] and the diffusion of gas through liquid,

$$J(R) = -D\nabla C\big|_R = 2DA/R^2 = \alpha\left(HC_b - C(R)\right) \tag{79}$$

$$\Rightarrow A(R) = \frac{\alpha HR}{DR_gT} \cdot \frac{2\gamma + pR}{1 + \alpha R/D}. \tag{80}$$

From conservation of mass/particles, the change in molecules inside the bubble is equal to the total outflux,

$$\frac{d}{dt}\left(VC_b\right) = -\int_S JdS = S \cdot J = 4\pi R^2 J(R), \tag{81}$$

where S is the surface of the bubble. By inserting equation [80] and equation [7], that is assuming instantaneous mechanical equilibrium, into [81] and rearranging, an ODE for the radius can be found,

$$\dot{R} = -3\alpha H \left(\frac{2\gamma + pR}{4\gamma + 3pR}\right) \cdot \frac{1}{1 + \alpha R/D}. \tag{82}$$

As R goes to zero ($R \ll \gamma/p$ and $R \ll D/\alpha$), the ODE can be simplified to

$$\dot{R} \approx -3\alpha H. \tag{83}$$

It is also possible to calculate the analytical solution of equation [82] with integration by substitution ($u = 1 + p_f R/(2\gamma)$), and assuming initial conditions $R(t = 0) = R_0$ and $t = 0$,

$$t = \frac{-1}{3\alpha H}\left[\left(\frac{4\gamma^2\alpha}{Dp_f^2} - \frac{2\gamma}{p_f}\right)\ln\left(\frac{2\gamma + Rp_f}{2\gamma + R_0 p_f}\right) + \left(3 - \frac{2\gamma\alpha}{Dp_f}\right)(R - R_0) + \frac{3\alpha}{2D}\left(R^2 - R_0^2\right)\right]. \tag{84}$$

In the case of where α goes to infinity, the rate of which the gas can dissolve is so rapid that the concentration at the boundary will be in equilibrium with the gaseous phase according to Henry's law, and the expression for A now becomes,

$$C(R) = HC_b \tag{85}$$

$$\Rightarrow J(R) = \frac{DH}{RTR_g}\left(2\gamma/R + p\right). \tag{86}$$

Equation [81] still holds, and by inserting equations [86] and [7], and rearranging and ODE for the radius can be found,

$$\dot{R} = -\frac{3DH}{R}\left(\frac{2\gamma + Rp}{4\gamma + 3pR}\right). \tag{87}$$

Similarly, when $R \ll \gamma/p$, the ODE can be simplified to

$$2R\dot{R} \approx 3DH. \tag{88}$$

The analytical solution of equation [87] with the same initial conditions as in the case where α goes to zero can be calculated to be,

$$t(R) = -\frac{4\gamma^2}{p_f^2}\ln\left(\frac{2\gamma + Rp_f}{2\gamma + R_0 p_f}\right) + \frac{2\gamma}{p_f}(R - R_0) - \frac{3}{2}\left(R^2 - R_0^2\right). \tag{89}$$

3.7 Numerics and computational specifications

The computer used is a Lenovo Think Pad x220i, with an INTEL i3-2350M CPU with 2.3 GHZ processor and 4 GB RAM. The executional time of the algorithm for a curved boundary condition for one iteration is of order seconds, and the executional time for an steady state solution will depend on the starting conditions for the bijection. For typical parameters there is a need of 10-12 iterations, and the execution time will therefore be of an order of $\mathcal{O}(10)$s.

4 Results

4.1 Flat bubble

In the flat bubble approximation, an electrode of a 100 nm is partially covered with a bubble with an imposed radii. A flux is then imposed on the system, and the concentration profile for a bubble the system can be calculated. Two examples are illustrated in figures 11 and 12.

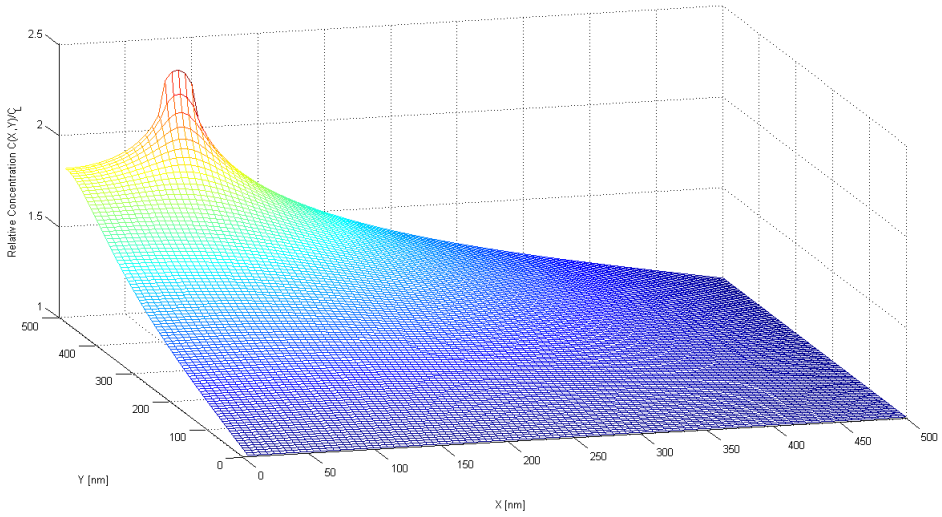

Figure 11: Relative hydrogen concentrations distribution, with radii 75nm, and flux 0.1 mol/sm^2 from a partially covered electrode of a 100nm.

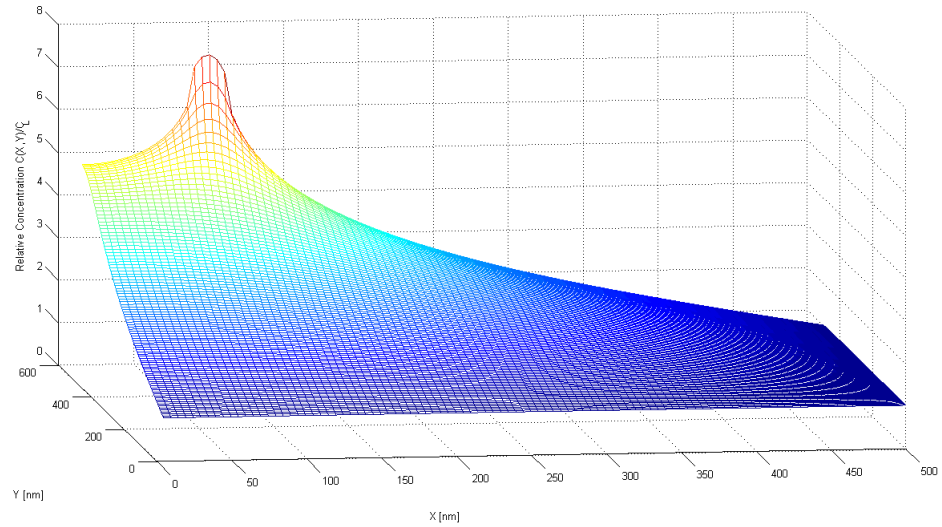

Figure 12: Relative hydrogen concentration distribution, with radii 75nm, and flux 0.5 mol/sm^2 from a partially covered electrode of a 100 nm.

One sees that concentration of hydrogen spreads out in the liquid through diffusion, and thus is falls off as the distance to the electrode increases. The flux of hydrogen between the liquid and the bubble can be evaluated through calculating the surface integral of equation [54] over the surface of the bubble. And from equation [55], the contact angle can be calculated for such a system. The contact angle as a function of the radius is shown in figure 13;

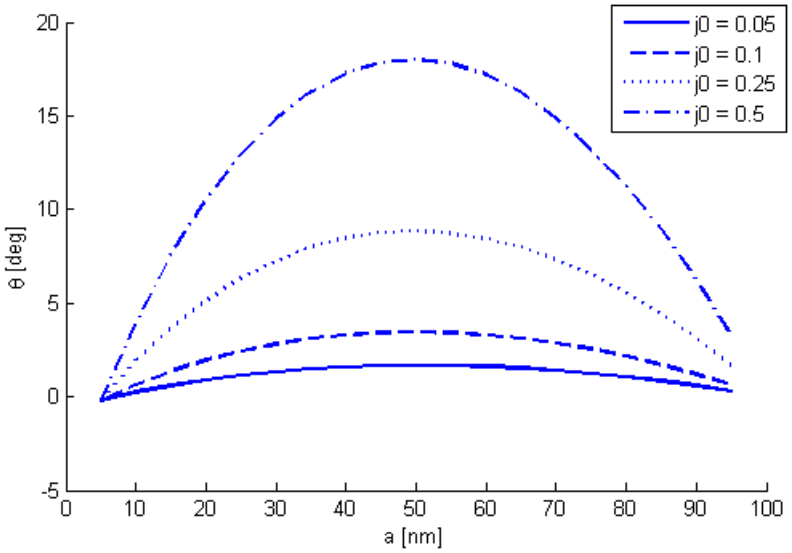

Figure 13: The contact angle [deg] as a function of the radii, with fluxes in the range of 0.05-0.1 mol/sm^2.

A negative contact angle is inconsistent with how the system is defined, is only arises from the way the contact angle is calculated in equation [55]. And it is therefore clear that the given concentration profile cannot upheld a nanobubble of the imposed radii, and the system is therefore not a steady state solution.

To investigate the properties of [55], the contact angle as a function of flux. Such cases is shown in figures 14 - 17.

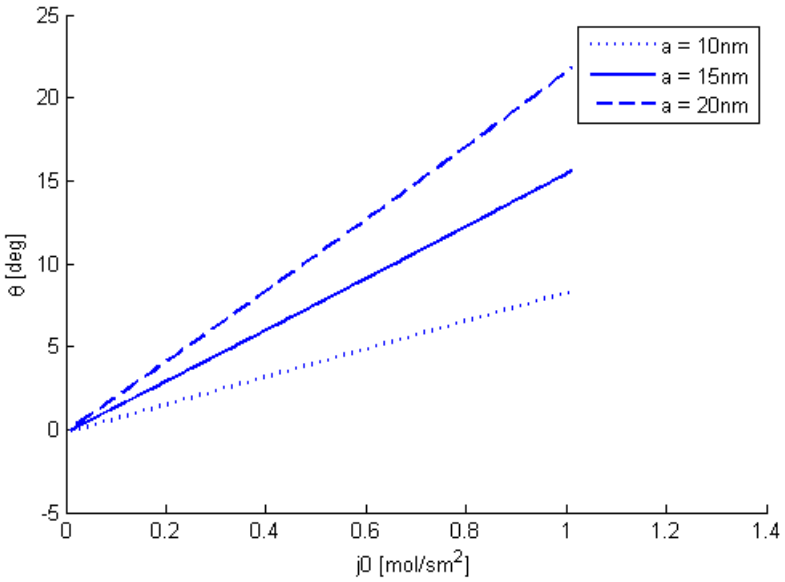

Figure 14: The contact angle [deg], as a function of the flux, at a constant radii.

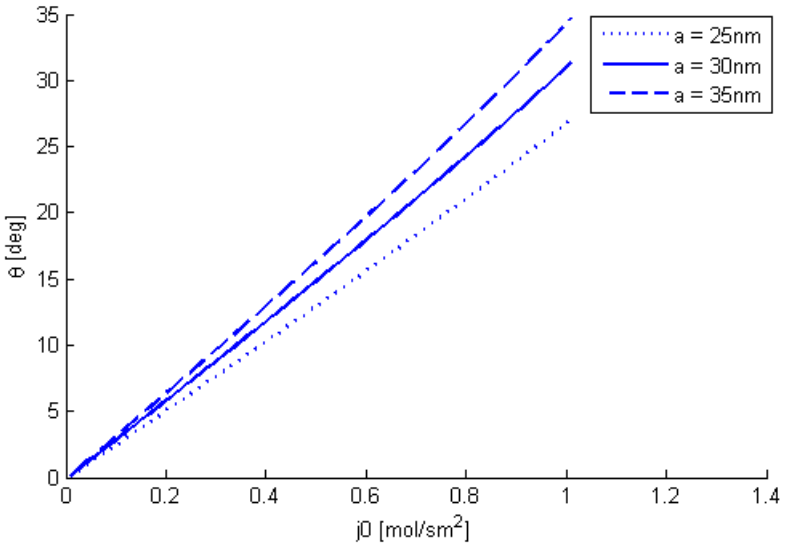

Figure 15: The contact angle [deg], as a function of the flux, at a constant radii.

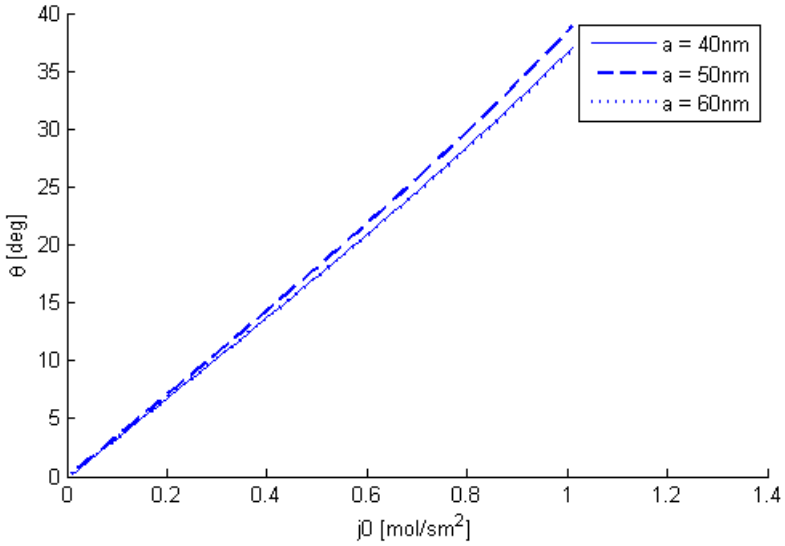

Figure 16: The contact angle [deg], as a function of the flux, at a constant radii.

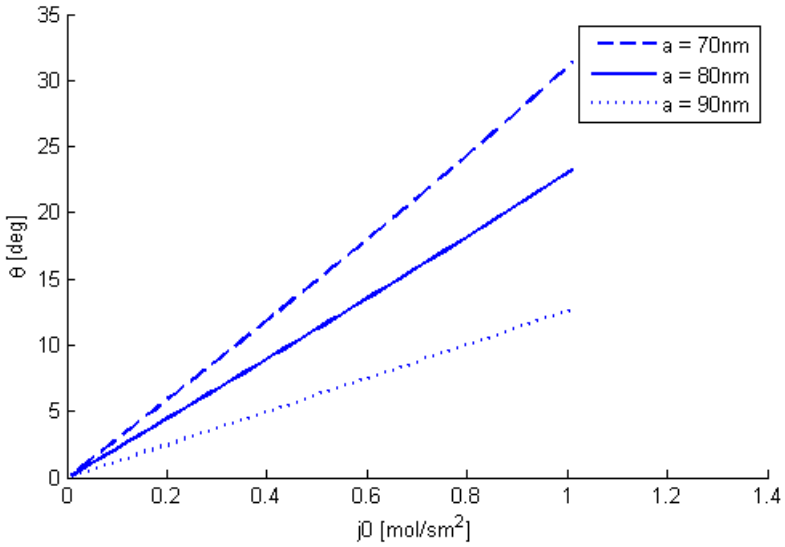

Figure 17: The contact angle [deg], as a function of the flux, at a constant radii.

The linear nature of the contact angles, is illustrated in figure 18. In the figure the calculated contact angle and a linear regression line is plotted. The regression is made for fluxes lower than 0.5 mol/sm^2, and for a bubble with radii 55 nm. The regression line has a slope of 0.0108 rad·s·m^2/mol.

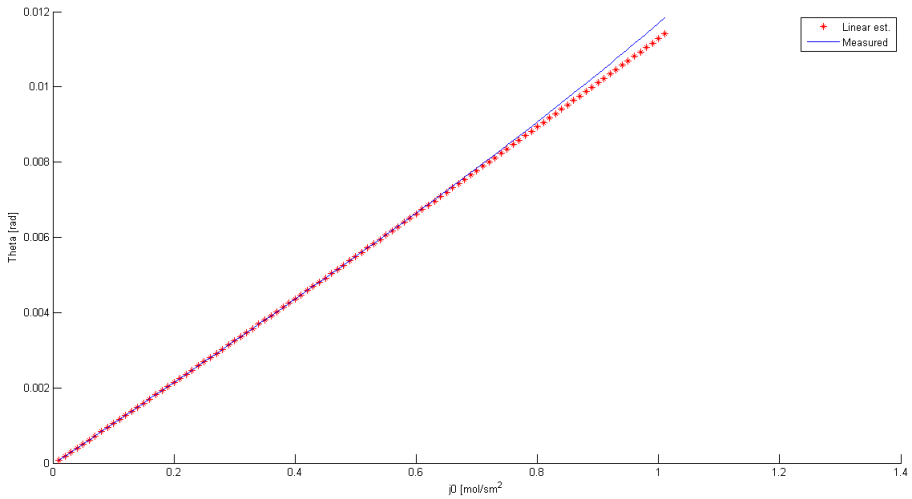

Figure 18: Linear estimation of a nanobubble with radii 55 nm. $\theta(j) = 0.0108j$ rad

4.1.1 Linear dependence

From the figures 14 - 17, one observes that the contact angle is nearly linear with respect to the flux, at least for small contact angles. It is well known that in a two-dimensional steady state diffusion with one of the Neumann boundary condition, the concentration at any fixed point in space is directly proportional to this imposed flux boundary condition. Thus the concentration of hydrogen along the surface of the bubble would be proportional to the imposed flux j_0. From equation [7] it is observed that concentration in the bubble at a fixed radii, is proportional to $\sin(\theta)$, and by equations [10] and [54] it is observed that the flux at any point along the boundary is dependent on the concentration differences along the surface of the bubble. It is therefore expected that the imposed flux on the electrode for a steady state solution should be proportional to $\sin(\theta)$ for a fixed radii.

It is well known that at small angles, one can approximate $\sin(\epsilon) \approx \epsilon$. The plots is obviously shown in degrees, but this is only a scaling factor between the units for degrees and radians. And as indicated by figure 18 the linear dependence is decreasing as the flux increase. By applying common values for the system to equation [55], it is easy to approximate $\theta \sim 10^{-2} j_0$ rad, which is in good agreement with the slope of the linear estimation shown in figure 18.

4.2 Curved surface

When the bubble surface is included and a flux boundary condition along the bubble, the steady state concentration profile for a nanobubble with an imposed radii and contact angle can be calculated, and illustrated in figures 19 - 22.

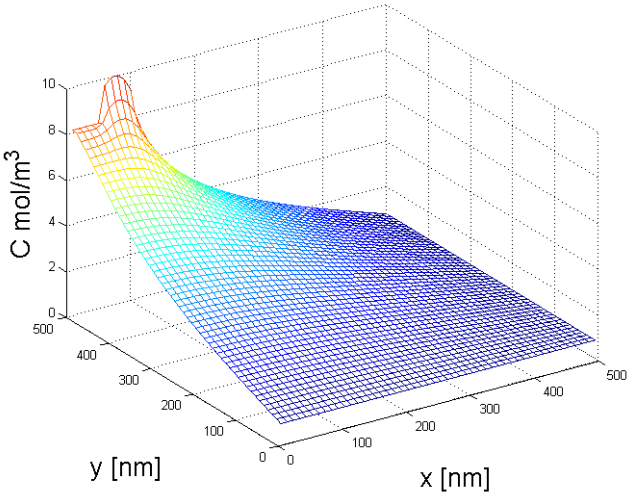

Figure 19: The concentration profile of hydrogen through the domain of 500×500nm, for a surface bubble with $\theta = 20\,\text{deg}$ and radii $a = 50$ nm. The electrode is located at $x = 0 - 100$ and $y = 500$, that is the top left corner. The bubble covers the electrode from $x = 0$ to $x = a$nm, and the production of hydrogen occurs on the par of the electrode which is not covered by the bubble.

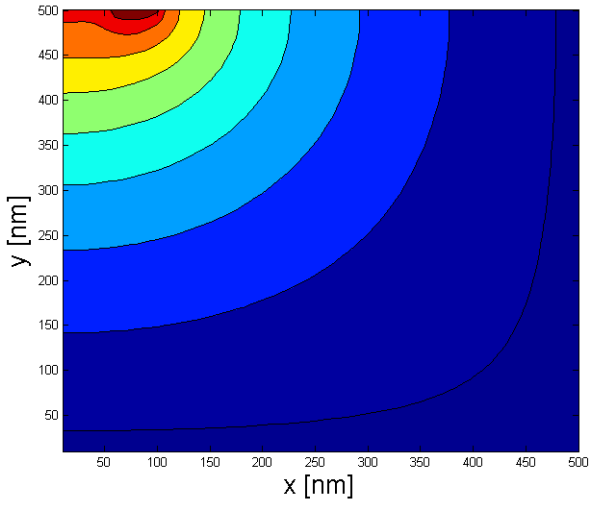

Figure 20: Contour-plot of the concentration profile of hydrogen through the domain of 500×500nm, for a surface bubble with $\theta = 20\,\text{deg}$ and radii $a = 50$ nm. The electrode is located at $x = 0 - 100$ and $y = 500$, that is the top left corner. The bubble covers the electrode from $x = 0$ to $x = a$nm, and the production of hydrogen occurs on the par of the electrode which is not covered by the bubble.

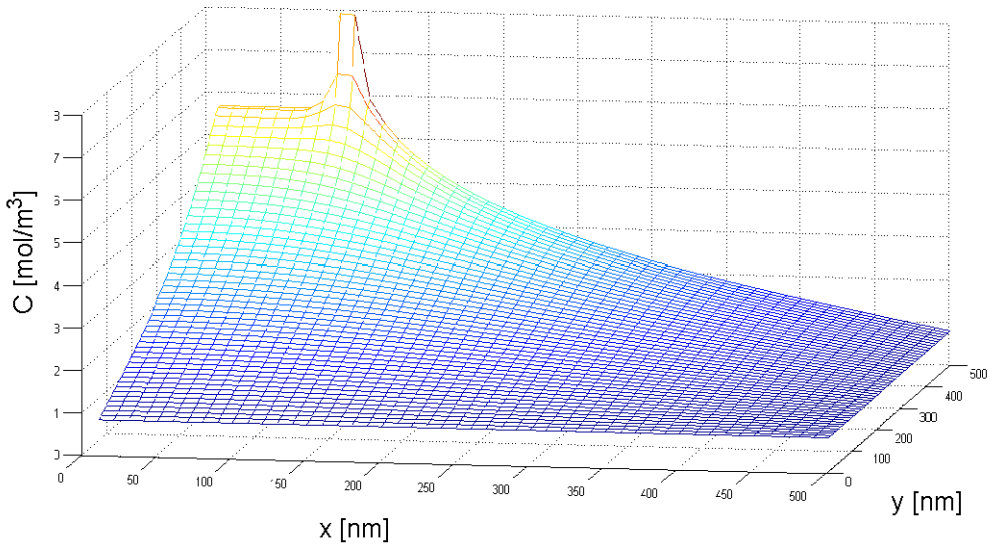

Figure 21: The concentration profile of hydrogen through the domain of 500 × 500nm, for a surface bubble with $\theta = 20\,\text{deg}$ and radii $a = 75$ nm. The electrode is located at $x = 0 - 100$ and $y = 500$, that is the top left corner. The bubble covers the electrode from $x = 0$ to $x = a$ nm, and the production of hydrogen occurs on the par of the electrode which is not covered by the bubble.

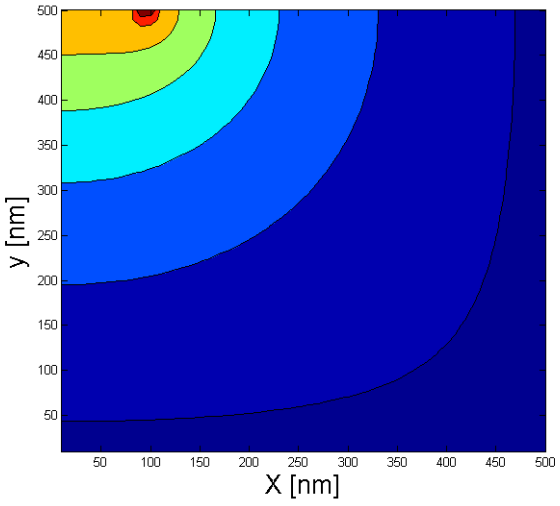

Figure 22: Contour-plot of the concentration profile of hydrogen through the domain of 500 × 500nm, for a surface bubble with $\theta = 20\,\text{deg}$ and radii $a = 75$ nm. The electrode is located at $x = 0 - 100$ and $y = 500$, that is the top left corner. The bubble covers the electrode from $x = 0$ to $x = a$nm, and the production of hydrogen occurs on the par of the electrode which is not covered by the bubble.

The contact angle is a material dependent quantity, so it can be expected that for a system with given gas, liquid and solid phases, the contact angle would be constant. Further there is also expected that the as the flux between the liquid and the vapour is proportional to α, the production of hydrogen may depend on α. The flux from the electrode j_0 for a stable bubble with given contact angles in the range $7.5 - 32.5$ deg, is shown as a function of the radii of the bubble for α in the range of $0.01 - 1$ m/s in figures 23 - 31

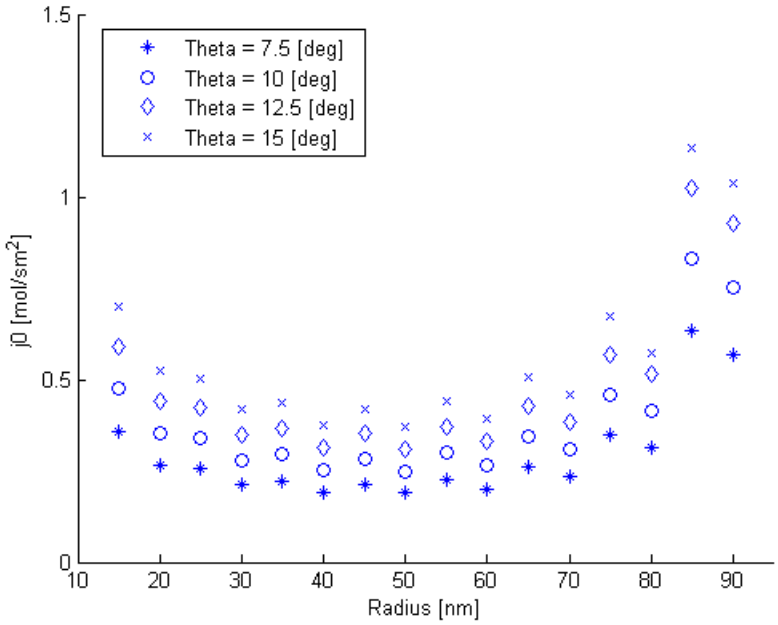

Figure 23: The needed influx j_0 as a function of the contact angle for $\alpha = 0.1$

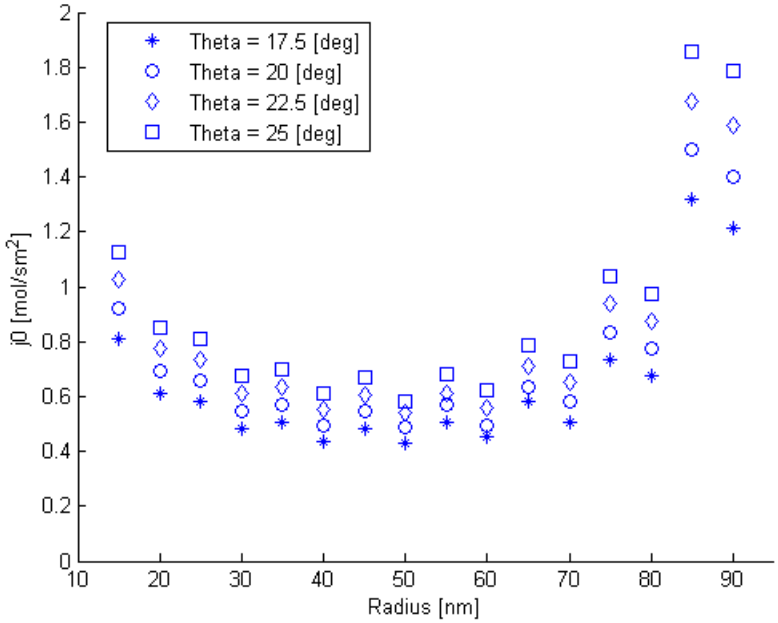

Figure 24: The needed influx j_0 as a function of the contact angle for $\alpha = 0.1$

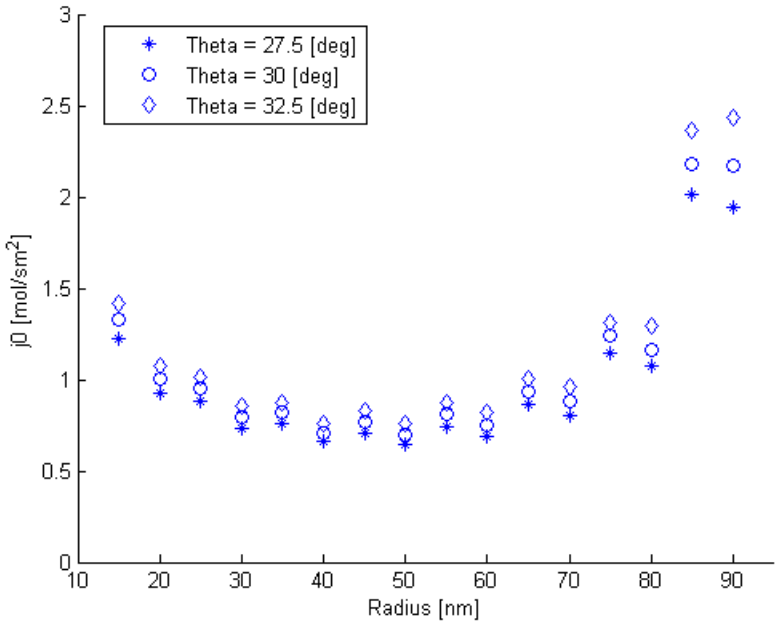

Figure 25: The needed influx j_0 as a function of the contact angle for $\alpha = 0.1$

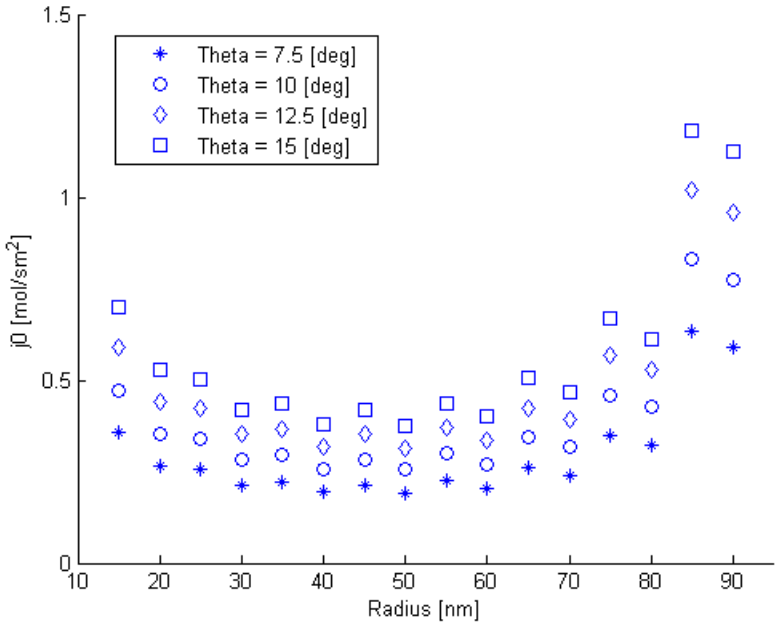

Figure 26: The needed influx j_0 as a function of the contact angle for $\alpha = 0.01$

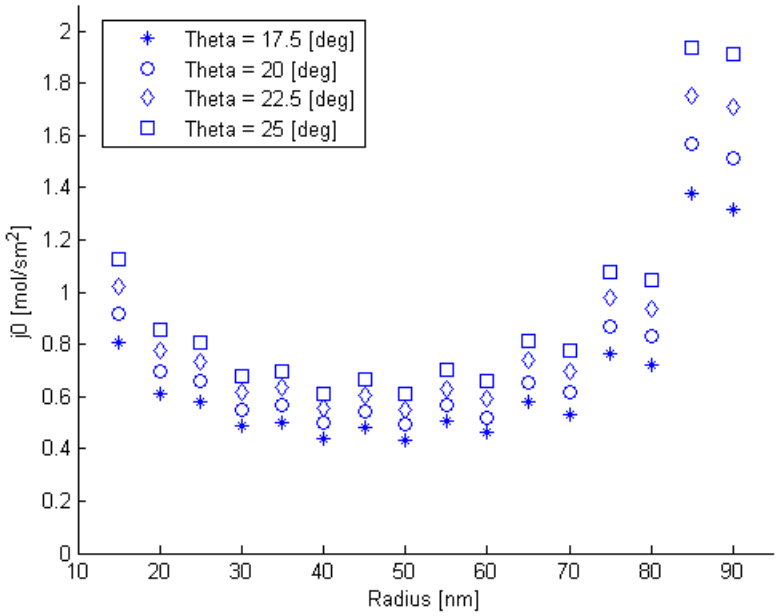

Figure 27: The needed influx j_0 as a function of the contact angle for $\alpha = 0.01$

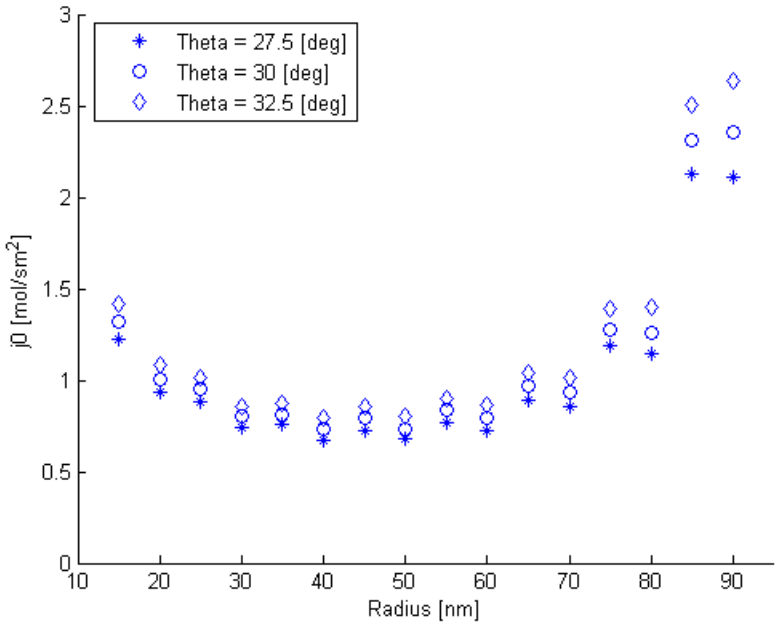

Figure 28: The needed influx j_0 as a function of the contact angle for $\alpha = 0.01$

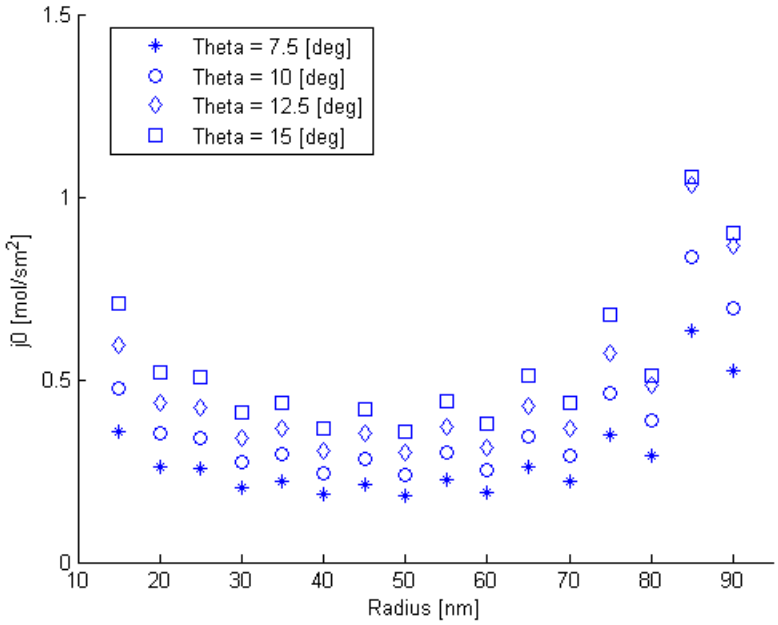

Figure 29: The needed influx j_0 as a function of the contact angle for $\alpha = 1$

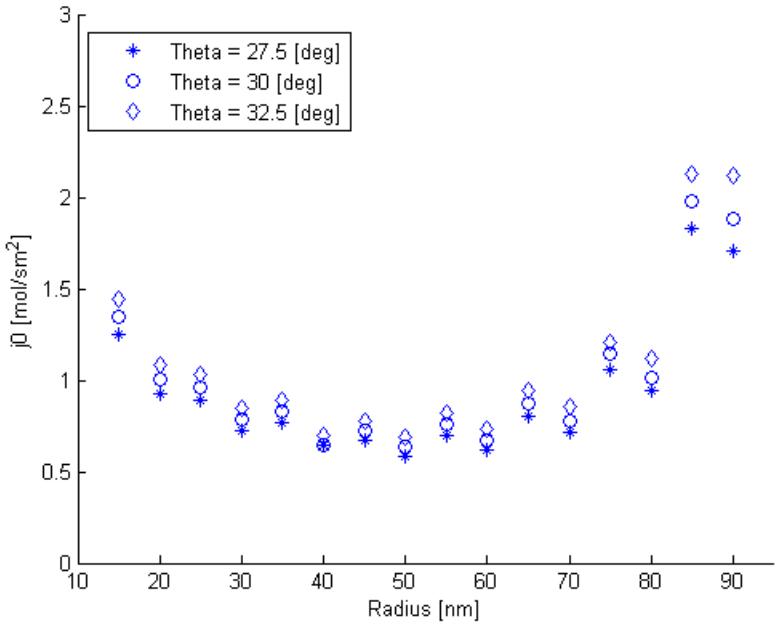

Figure 30: The needed influx j_0 as a function of the contact angle for $\alpha = 1$

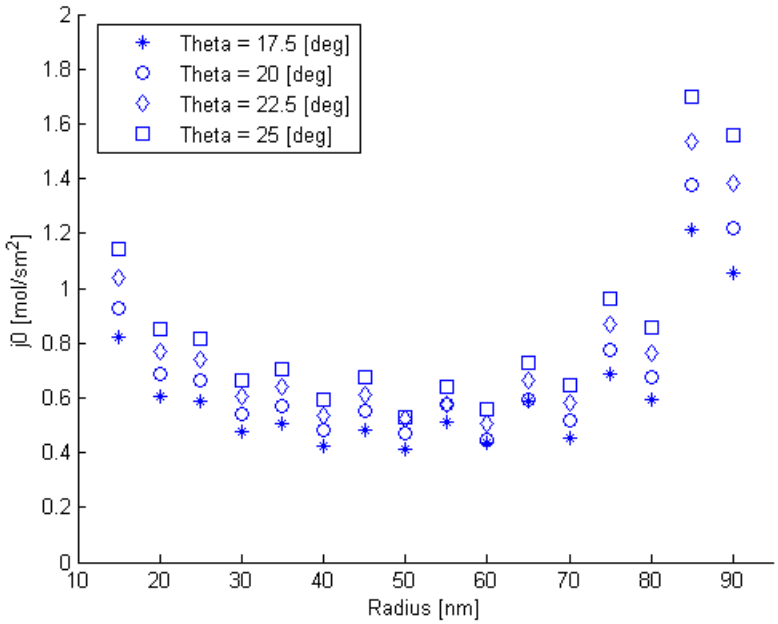

Figure 31: The needed influx j_0 as a function of the contact angle for $\alpha = 1$

The overall form of the flux j_0 is as expected. Where at small radices the concentration in the bubble will be high, and thus a high concentration along the surface of the bubble is needed to be close to equilibrium. As the radii is increased whilst the contact angle remains constant the concentration decreases, and thus the concentrations along the bubble surface

will have to be decreased in order for the system to be at a steady state. As the radii is increased, the area of the electrode where hydrogen production can occur decreases and therefore when the bubble covers a large part of the electrode and the net influx of hydrogen is decreased for a given j_0. Therefore for bubbles with large radices, a, approaches the length of the electrode, the flux per unit area has to be increased in order to achieve a concentration profile that yields a steady state solution. It is also worth noting that for a concentration profile that yields a nonzero flux between the liquid and gas phase, the system cannot be claimed to be at a steady state. Therefore a claim of either a bubble growth or reduction based on a net positive or negative flux.

As in the flat bubble approximation, a higher contact angle would yield a higher concentration inside the bubble and therefore a higher concentration along the surface of the bubble and thus the flux at the electrode has to be increased.

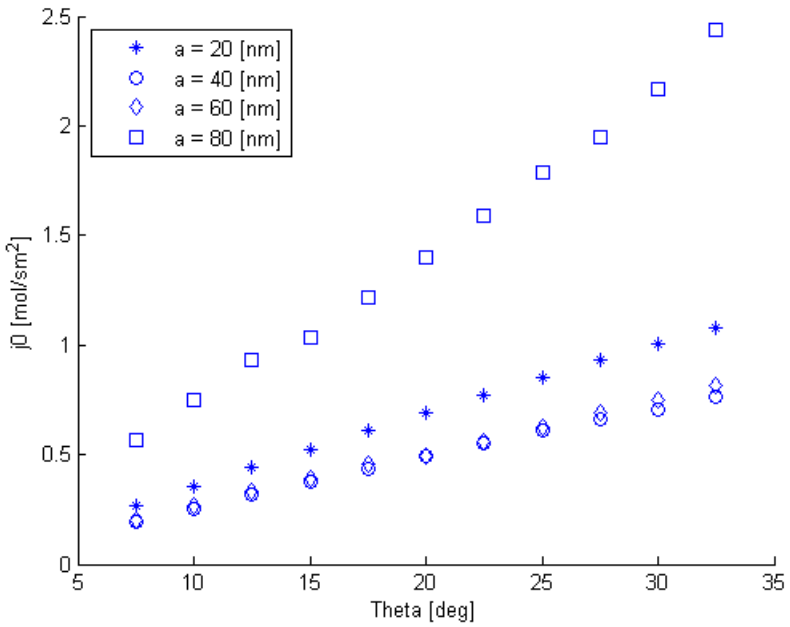

Figure 32: The imposed flux j_0 as a function of θ for a given radii with $\alpha = 0.1$.

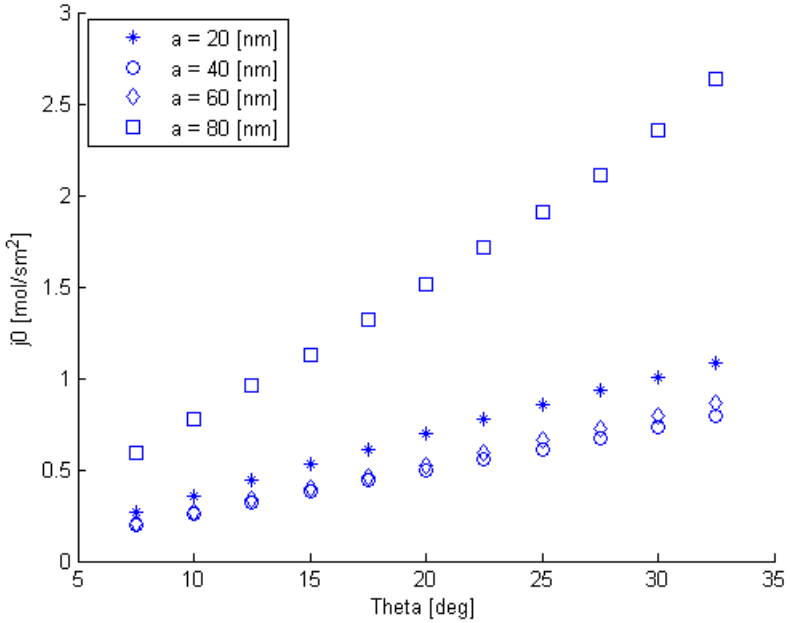

Figure 33: The imposed flux j_0 as a function of θ for a given radii with $\alpha = 0.01$.

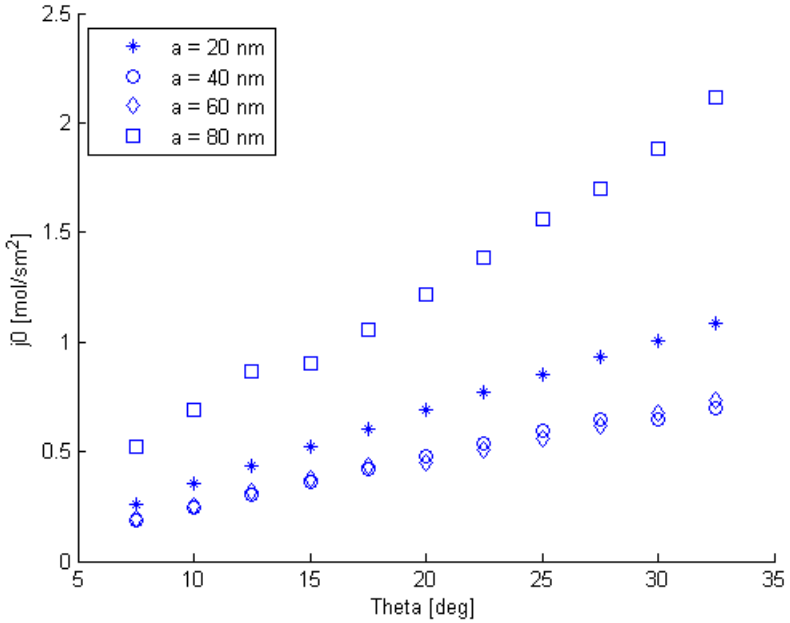

Figure 34: The imposed flux j_0 as a function of θ for a given radii with $\alpha = 1$.

The same linear dependence between the flux and the contact angle is observed for the curved surface as in the flat bubble approximation.

4.3 Estimation of α

The effect of α is illustrated in figure 35-36.

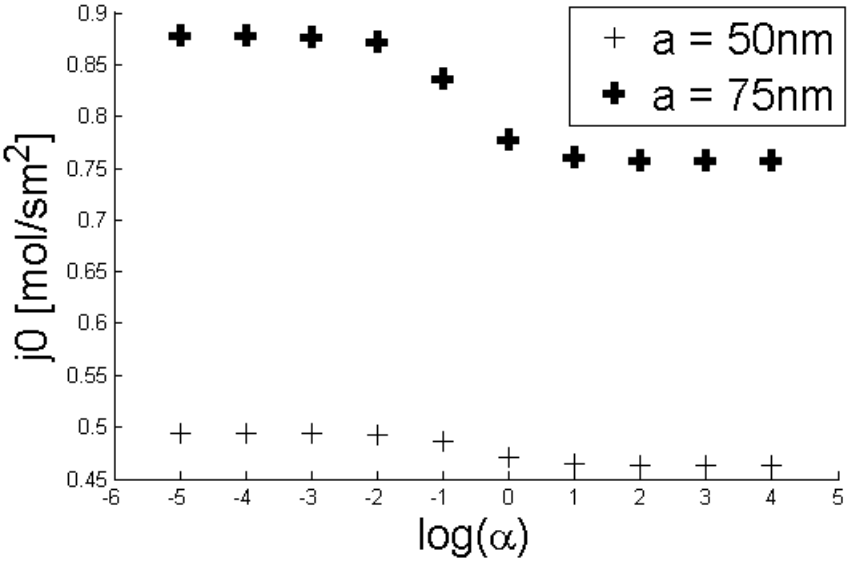

Figure 35: The flux j_0 as a function of α for a stable nanobubble with $\theta = 20\,\text{deg}$ and radii of 50 and 75 nm. The x-axis is the common logarithm (base of 10) of α witch varies from 10^{-5} to 10^4

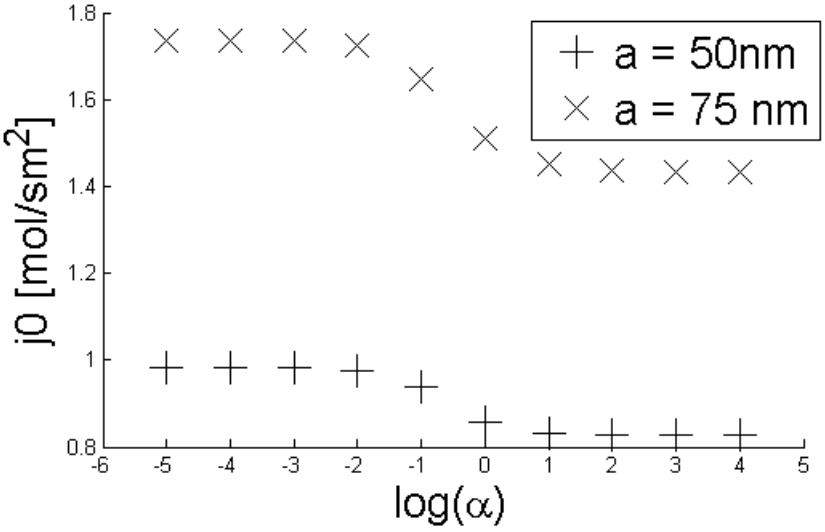

Figure 36: The flux j_0 as a function of α for a stable nanobubble with $\theta = 40\,\text{deg}$ and radii of 50 and 75 nm. The x-axis is the common logarithm (base of 10) of α witch varies from 10^{-5} to 10^4

As α goes to zero, the flux converges to a towards a constant value. This is to be expected, because in the limit $\alpha \to 0$, the boundary condition along the surface of the

bubble becomes a Neumann boundary condition. Therefore all concentration profiles will be independent of α, and only depend on the imposed flux and the geometry the bubble. The bubble covers parts of the electrode, so the net influx of hydrogen into the system will depend on the radii of the bubble and the concentration of gas inside the bubble depend on the contact angle. The diffusion of hydrogen away from the electrode will be restricted by the area of the domain which the bubble covers. Thus for any imposed flux and bubble geometry, the calculated concentration profiles will be the solution of the steady state diffusion equation in two dimensions with mixed boundary conditions.

Any calculated concentration profile cannot be claimed to be a steady state solution, as the net flux across the boundary of the bubble will have to be zero for all time-derivative of the system to zero. So the steady state solution of the system is the concentration profile that yields a net flux of zero across the boundary of the bubble. From [10] it is observed that the net flux is proportional to α, and as the concentration profiles are independent of α, the problem becomes simply to find the concentration profile where the integral of weighted concentration differences, $C_{aq} - HC_b$, is zero. As the concentrations is independent of α, so will the needed imposed flux j_0 be. An example for concentration along the surface of the bubble for small α are shown in figure 37

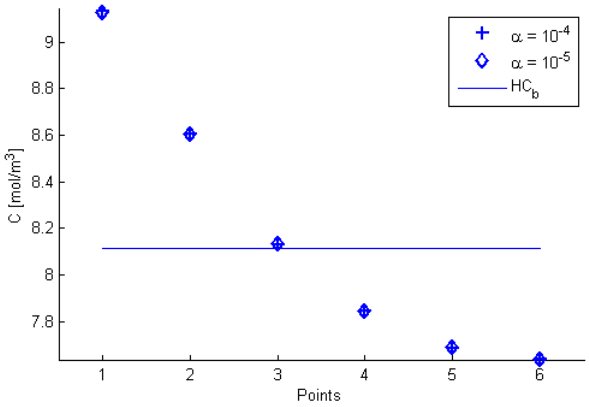

Figure 37: The concentration of dissolved hydrogen along the boundary of the bubble for small α, $\alpha = 10^{-4}$ and 10^{-5}.

In the other extreme case, where *alpha* goes to infinity, the boundary condition becomes a Dirichlet boundary condition. At the limit $\alpha \to infty$, the concentrations along the boundary has to be in equilibrium with the bubble in order for not have an infinite flux between the phases. At as α becomes large, the concentrations along the boundary will have to be near the equilibrium concentration $C_{aq} \approx HC_b$ in order for the fluxes to be of reasonable values. Therefore the calculated concentration profiles will be independent of α, and is determined only by the imposed influx, j_0. And thus the steady state solution is the concentration profile that yields a zero net flux across the boundary, which is the imposed flux that yields that the concentration along the bubble is close to the weighted concentration in the bubble. Some values for the concentration is shown in figure 38.

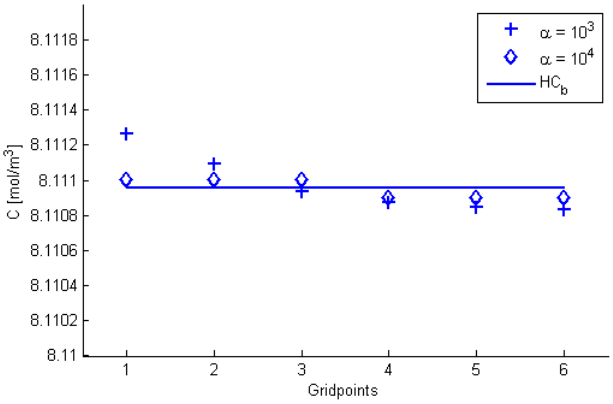

Figure 38: The concentration of dissolved hydrogen along the boundary of the bubble for large α, $\alpha = 10^3$ and 10^4.

From equation [73], it is clear that Dirichlet term of Robin boundary condition for the bubble is proportional to $\alpha\Delta x/D \approx \alpha$, and the Neumann boundary contrition is of $\mathcal{O}(1)$. When α becomes small, $\alpha < 10^{-2}$, the Dirichlet term becomes negligible. In the other extreme where α becomes large, $\alpha > 10^2$ the Dirichlet term of the Robin boundary condition becomes negligible. The concentrations of dissolved gas along the surface has to be in chemical equilibrium with the gaseous phase. From equation 1, it is clear that the flux is proportional to the concentration gradient. At the limit where α becomes large, the concentrations along the bubble will be almost constant.

It can also be observed that the range of which the boundary condition along the surface of the bubble is dependent on the diffusion constant D. And by varying the diffusion constant the area of which the evaporation rate constant affects the solution would shift. This effect is shown in figures 39 - 40.

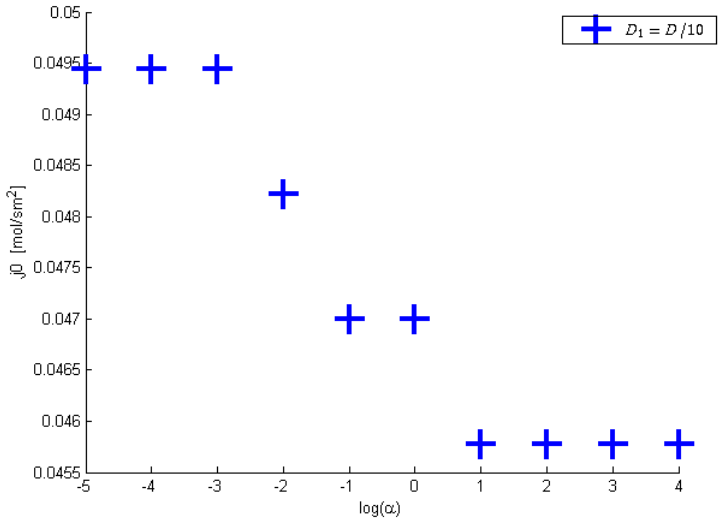

Figure 39: The flux j_0 as a function of the common logarithm of α for a stable nanobubble with $\theta = 20\,\text{deg}$ and radii of 50 nm with diffusion constant $0.1D$.

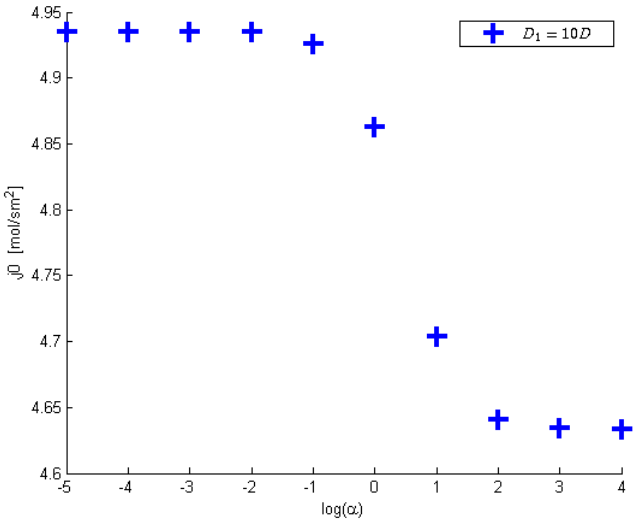

Figure 40: The flux j_0 as a function of the common logarithm of α for a stable nanobubble with $\theta = 20\,\text{deg}$ and radii of 50 nm with diffusion constant $10D$. The regimes of which where the flux becomes independent is shifted to the right

The observed effect is as expected, when the diffusion constant is change by an order of 10, the domain of which the evaporation rate constant affects the system is increased by an order of 10. Similar if the diffusion constant is reduced by an order of 10, the area of which the evaporation rate constant affects the system is decreased by an order of 10. As diffusion constant is the proportionality constant between the molar flux due to molecular diffusion and the gradient in the concentration, it is expected that the influx will have to be increased for high values of D, and decreased for low values of D. This effect is seen in figures 39 - 41.

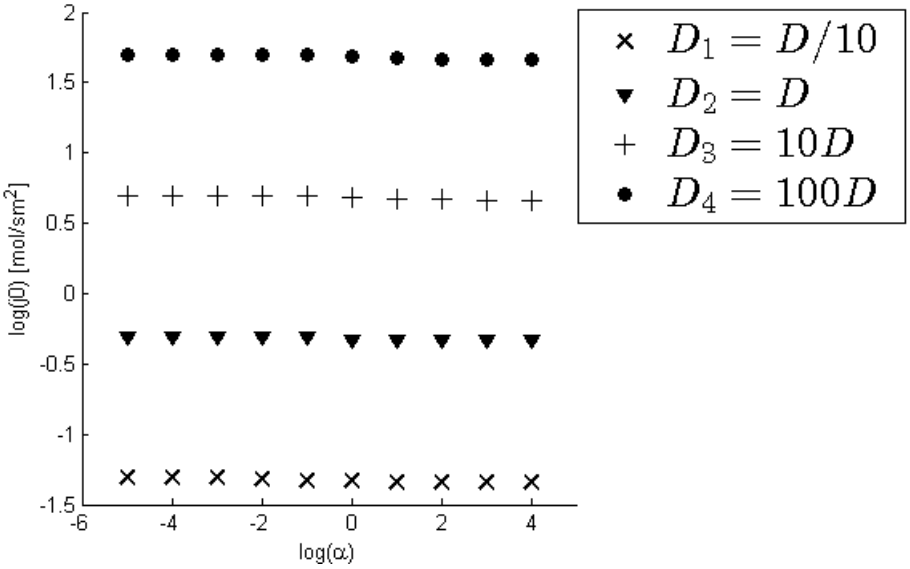

Figure 41: The common logarithm of the flux j_0 as a function of the logarithm α for a stable nanobubble with $\theta = 20\,\text{deg}$ and radii of 50 nm with various diffusion constants. The flux scales proportional to the diffusion constant.

The value of α can be estimated from the paper by Brenner and Lohse [3] [figure [2]], where the volume flux between a bubble and the liquid is found to be of an order of $3{\cdot}10^{-16}$ m^3/s. By applying typical values for the concentrations in this two dimensional domain, an estimation of α can be found by applying equation [10]. In this model the difference of typical weighted concentration for the bubble, HC_b, and hydrogen concentrations in the liquid will be of $\mathcal{O}(1)$ mol/m^3. To approximate the volume flux, the flux has to be divided by the area of the surface of the spherical cap, $S = 2\pi Rh$. By comparing this estimate with the results from Brenner and Lohse, α is found to be of an order of $\mathcal{O}(10^{-1})\text{m}/\text{s}$.

4.4 Simple model of bulk nanobubble

As derived in equation [84] the dissolution-time of a bulk nanobubble in the limit $\alpha \to 0$ can be calculated. The radii of the bubble can be calculated as a function of the time, and is shown in figure 42.

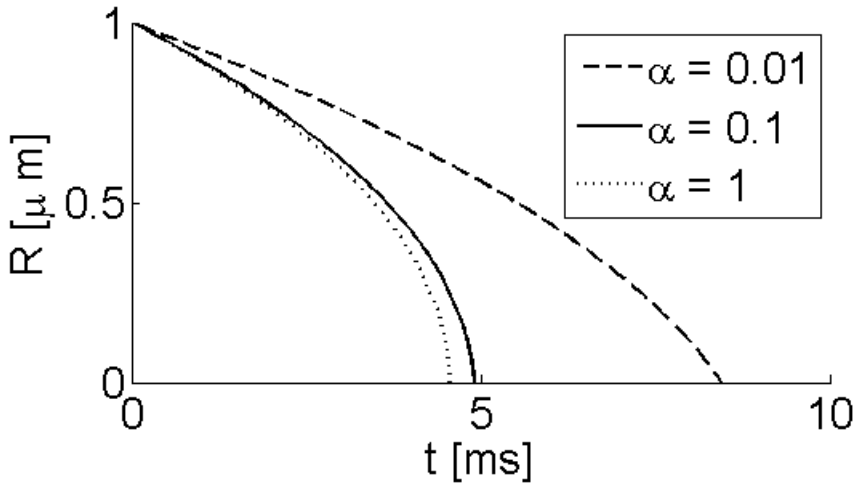

Figure 42: The radii of a bulk nanobubble as a function of the time for α in the range $10^0 - 10^{-2}$. The characteristic time scale of the dissolution-time is observed to be of order ms.

From [84] and [83] it is observed that for for small α, the characteristic time scale for the dissolution is inversely proportional to α, $\tau \propto 1/(H\alpha)$. For typical values the expected dissolution-time will the be of order ms, as shown in 42. With this simple model it is then shown that the dissolution time will depend on α, and if the evaporation rate constant is small, the dissolution time will increase by several orders of magnitude compared to classical diffusion theory. [3]

The dissolution-time of a bulk nanobubble in the limit $\alpha \to \infty$, can be calculated using [89], and the radii as a function of time is shown in 43.

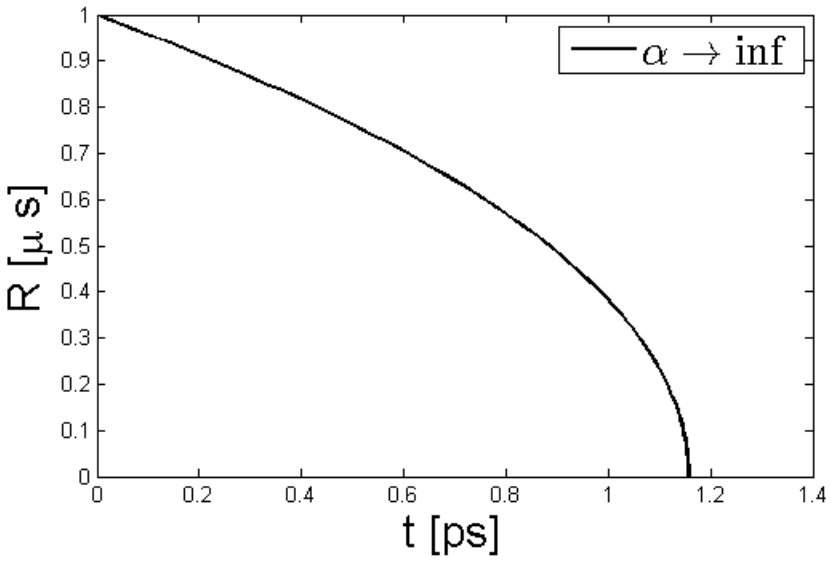

Figure 43: The radii of a bulk nanobubble as a function of time for the limit $\alpha \to \infty$. The observed characteristic time scale of the dissolution-time is observed to be of order ps.

From equations [89] and [88] it is observed that for large α the characteristic time scale for dissolution is proportional to the diffusion constant, $\tau \propto HD$, and thus the dissolution time would for typical values be of order ps. As the concentration near the surface of the bubble will be in constant chemical equilibrium with the vapour, and as the concentration inside the bubble is inversely proportional to the radii R.

5 Outlook

5.1 Flat bubble approximation

The flat bubble approximation is a crude model to of which is only valid for bubbles with very low contact angle. When the contact angle becomes to large the assumptions made becomes to inaccurate. The surface integral does not account for the fact that the surface is longer than the radii of the bubble by a factor of $\sin(\theta)$, and the imposed boundary conditions will not account for the fact that the boundary is closer to some points, or even inside when the bubble height is larger than the grid size, as in the model for the curved boundary model. However as demonstrated in 35 the boundary condition of no flux along the surface of the boundary is appropriate for a low alpha.

5.2 Three dimensional model

There are some problem regarding mass conservation in two dimensions, as the solution of the steady state diffusion equation in two dimensions will depend on the size of the domain considered. If the domain considered were to be increased, with the same boundary condition, the concentrations at the flux boundary condition would have to increase in order to not achieve a nonzero concentration at the other boundary.

To use a finite difference scheme in three dimensions can be justified, however to implement a curved boundary condition with finite difference in three dimensions is extremely cumbersome. And would probably be more work and less accurate than to apply a finite elements or finite volume scheme. There would also be needed a greatly larger amount of points to span the bubble surface and therefore also an even greater increase the execution time. The number of calculations needed to solve the problem will be greatly increased. If the size of the problem were to be expanded with a new dimension with equal size, the number of equations and unknown will then be increased by a factor of n. The matrix for the problem will increase from a $n^2 \times n^2$ in two dimensions, to $n^3 \times n^3$ in three dimensions. And is well known that the inversion algorithm of a matrix of size $m \times m$, will have an complexity $\mathcal{O}(m^3)$, e.g Gauss-Jordan elimination (there are however some methods that reduces the complexity of the inversion). The execution time will therefore be greatly increased, $\mathcal{O}(n^6) \rightarrow \mathcal{O}(n^9)$.

5.3 Error estimations

The finite difference scheme will for all points, except points involving the curved boundary, be second order accurate. To analyse the truncation error for the points involving curved boundary is not straightforward, but it should be noted that the truncation error may not tend to zero regardless of the definition of the mesh [9, Chapter 3.4, p77]

> These methods for approximating the curved boundary lead to truncation errors of lower order than those at ordinary internal points, especially where normal derivatives are involved. Just as we found in the one-dimensional case in Section 2.13, the truncation error may not tend to zero at these points when the mesh is refined. It is difficult to produce higher order approximations with the desirable properties. For example, we have used the simplest approximation to the normal derivative, incorporating just the two points U_B and U_Z. Now

suppose we extend the normal at B to the point R in Fig. 3.8, where $ZR = (q/\alpha)\Delta y$. Then a higher order approximation to the derivative is

$$g_b = \frac{\partial u}{\partial n} \approx \frac{(1+2\alpha)u_B + \alpha^2 u_R - (1+\alpha)^2 u_Z}{(1+\alpha)q\Delta y}$$

It will now be more awkward to interpolate for the value u_R, and moreover the coefficients of u_Z and u_R have opposite signs. The resulting scheme will not satisfy a maximum principle. It seems likely that such a higher order scheme will be unsatisfactory in practice unless further restrictions are imposed.

5.4 Thermodynamical consistent model

Even a better numerical scheme with an higher order of accuracy may not explain the longevity of the surface nanobubbles, an a thermodynamical consistent model may have to be applied. The system is assumed to be isothermal, and the electric potential of the ions is not taken into account. The system is neither model for a high pressure, which is often the case in electrolysis. [4], [8].

In this model it is model assumed that the bubble only consist of one gaseous phase, when there is really no reason this should be the case. Most of the theoretical work regarding nanobubbles that has been published makes the same assumption. There have however been some work done on a multiphase model[15]. Where a thermodynamical approach is used to study the nucleation of weak solutions of gas dissolved in a liquid, and how the pressure affects the nucleation. Their work on nucleation theory and the critical radii - the radii a nucleus must reach for a nucleus/bubble must exceed for it to be stable/grow, can be exploited. As there have not been much work on nanobubble assuming multiple phases in the gaseous domain, there is obviously great potential for breakthroughs.

The hydrogen vapour in the bubble is assumed to be well mixed, and the ideal gas law is used to calculate the concentration inside the bubble. It is well known that the ideal gas law neglects both molecular size and intermolecular attractions, and thus for a low temperatures or high pressures it becomes less accurate. The gas inside the bubble will also be of Knudsen type, when the mean free path for the molecules is less than the height of the bubble. Therefore collisions occur at the solid substrate or the gas/liquid interface, rather than with other molecules. The gas molecules inside the bubble will therefore have a preferred direction, upwards from the substrate, as some of the molecules would be dissolved at the liquid/gas interface but all of the molecules that collide with the solid substrate will be reflected. [13]

5.5 Moving boundary for bubble dissolution

The model for the three dimensional bulk bubble dissolution assumes that the speed of which the bubble surface move is negligible, this is not necessary true, as the concentration will change as the radii decrease. The general problem is known as a free boundary value problem or a Stefan problem, and will have to be solved by continuously tracking the surface. It can be solved by non implementing a set of dimensionless equations, and evolve the system for a time-series where the radii is mapped back to the dimensionless equations for each timestep. This is however beyond the scope of this thesis.

5.6 Bubble formation

Nanobubbles are also observed in a cluster formation [16]. This would obviously have an effect on the dissolution time, as the diffusive gas from each bubble is restricted by the outflux from other bubbles. The diffusion then becomes essentially one-dimensional, and therefore greatly increase the longevity of the bubbles.

6 Conclusion

The steady state approach indicates that a single nanobubble which partially covers an electrode of a 100 nm can be stable, as long as the electrogeneration of hydrogen is sufficient to balance the dissolution of hydrogen at near the cap of the bubble. The effect is experimentally observed by Luo and White [6].

The results indicate that the evaporation rate constant only affects the needed influx of hydrogen when it is in the range of 0.01-1m/s, for values outside this range the influx of hydrogen converges. This effect is explained from the fact that the steady state solution becomes independent of α outside this range. The needed production of hydrogen is found to have depend more on the geometry of the bubble, than the evaporation rate constant, as for the net flux between the vapour and liquid to be zero it the concentration cannot vary

A simple model for the dissolution of a bulk nanobubble, where the outflux is assumed proportional to the evaporation rate constant, shows that the dissolution time is proportional to αH for small values of the evaporation constant. The evaporation rate is estimated to be of order $\mathcal{O}(0.1)$, which yields an approximated dissolution time of order ms.

References

[1] Appendix a.

[2] Frano Barbir. Pem electrolysis for production of hydrogen from renewable energy sources. *Solar Energy*, 78(5):661–669, 2005.

[3] Michael P Brenner and Detlef Lohse. Dynamic equilibrium mechanism for surface nanobubble stabilization. *Physical review letters*, 101(21):214505, 2008.

[4] SA Grigoriev, AA Kalinnikov, P Millet, VI Porembsky, and VN Fateev. Mathematical modeling of high-pressure pem water electrolysis. *Journal of applied electrochemistry*, 40(5):921–932, 2010.

[5] Henri Lhuissier, Detlef Lohse, and Xuehua Zhang. Spatial organization of surface nanobubbles and its implications in their formation process. *Soft Matter*, 10(7):942–946, 2014.

[6] Long Luo and Henry S White. Electrogeneration of single nanobubbles at sub-50-nm-radius platinum nanodisk electrodes. *Langmuir*, 29(35):11169–11175, 2013.

[7] Yijin Mao and Yuwen Zhang. Nonequilibrium molecular dynamics simulation of nanobubble growth and annihilation in liquid water. *Nanoscale and Microscale Thermophysical Engineering*, 17(2):79–91, 2013.

[8] Francesco Marangio, Massimo Santarelli, and M Cali. Theoretical model and experimental analysis of a high pressure pem water electrolyser for hydrogen production. *International Journal of Hydrogen Energy*, 34(3):1143–1158, 2009.

[9] Keith W Morton and David Francis Mayers. *Numerical solution of partial differential equations: an introduction*. Cambridge university press, 2005.

[10] Nikolai D Petsev, M Scott Shell, and L Gary Leal. Dynamic equilibrium explanation for nanobubbles' unusual temperature and saturation dependence. *Physical Review E*, 88(1):010402, 2013.

[11] Lord Rayleigh. Viii. on the pressure developed in a liquid during the collapse of a spherical cavity. *The London, Edinburgh, and Dublin Philosophical Magazine and Journal of Science*, 34(200):94–98, 1917.

[12] H Rezaei Nejad, M Ghassemi, SM Mirnouri Langroudi, and A Shahabi. A molecular dynamics study of nano-bubble surface tension. *Molecular Simulation*, 37(01):23–30, 2011.

[13] James RT Seddon, Detlef Lohse, William A Ducker, and Vincent SJ Craig. A deliberation on nanobubbles at surfaces and in bulk. *ChemPhysChem*, 13(8):2179–2187, 2012.

[14] Endre Süli and David F Mayers. *An introduction to numerical analysis*. Cambridge university press, 2003.

[15] CA Ward, A Balakrishnan, and FC Hooper. On the thermodynamics of nucleation in weak gas-liquid solutions. *Journal of Fluids Engineering*, 92(4):695–701, 1970.

[16] Joost H Weijs and Detlef Lohse. Why surface nanobubbles live for hours. *Physical review letters*, 110(5):054501, 2013.

[17] Shangjiong Yang, Peichun Tsai, E Stefan Kooij, Andrea Prosperetti, Harold JW Zandvliet, and Detlef Lohse. Electrolytically generated nanobubbles on highly orientated pyrolytic graphite surfaces. *Langmuir*, 25(3):1466–1474, 2009.

[18] Lijuan Zhang, Yi Zhang, Xuehua Zhang, Zhaoxia Li, Guangxia Shen, Ming Ye, Chunhai Fan, Haiping Fang, and Jun Hu. Electrochemically controlled formation and growth of hydrogen nanobubbles. *Langmuir*, 22(19):8109–8113, 2006.

7 APPENDIX A

7.1 Lagrange interpolating polynomial

The Lagrange interpolating polynomial, p_n, is the polynomial of degree $\leq n-1$ that passes trough the n-points (x_i, y_i), where $y_i = f(x_i)\ \forall i \in [1, n]$, it is given by

$$p_n(x) = \sum_{j=1}^{n} L_j(x) y_j, \tag{90}$$

$$L_j = \prod_{k=0, k\neq j}^{n} \frac{x - x_k}{x_j - x_k}. \tag{91}$$

A polynomial is trivial to integrate, and an approximation for the integral of the function $f(x)$ can be easily obtained

$$\int_a^b f(x)dx \approx \int_a^b p_n(x)dx \tag{92}$$

It can also be useful to define so called quadrature weights w_k, $k = 0, 1, ..., n$

$$w_k = \int_a^b L_k(x)dx \tag{93}$$

$$\Rightarrow \int_a^b f(x)dx \approx \sum_{k=0}^{n} w_k f(x_k). \tag{94}$$

7.2 Error estimation of trapezoidal rule

The trapezoidal rule (between two points a, b (linear estimation)) would be the same as estimating the integral with a Lagrange interpolating polynomial of degree 1. The trapezoidal can then be obtained as,

$$p_1(x) = L_0(x)f(a) + L_1(x)f(b), \tag{95}$$

$$\int_a^b f(x)dx \approx \int_a^b p_1(x)dx = \frac{b-a}{2}(f(a) - f(b)) \tag{96}$$

The error of this is defined by

$$E_n(f) = \int_a^b f(x)dx - \sum_{k=0}^{n} w_k f(x_k) \tag{97}$$

There exists is a theorem [14, p204, theorem 7.1] that states: Let $n \geq 1$ and f be a continuous real-valued, function defined on the interval $[a, b]$, and let $f^{(n+1)}$ be defined. Then

$$|E_n(f)| \leq \frac{M_{n+1}}{(n+1)!} \int_a^b |\pi_{n+1}| dx, \tag{98}$$

$$\text{Where } M_{n+1} = \max_{\zeta \in [a,b]} |f^{(n+1)}(\zeta)| \text{ and } \pi_{n+1} = (x - x_0)...(x - x_n). \tag{99}$$

By applying this theorem to the trapezoidal rule, in where $n = 1$ and $\pi = (x-a)(x-b)$, we find,

$$|E_1(f)| \leq \frac{M_2}{2} \int_a^b |(x-a)(x-b)| dx = \frac{(b-a)^3}{12} M_2. \tag{100}$$

By applying the same approach in the composite case, one can estimate the error in each step of the trapezoidal rule and summarize,

$$\mathcal{E} = \int_a^b f(x)dx - h\left[f(x_0)/2 + f(x_1) + ... + f(x_{N-1}) + f(x_N)/2\right] \tag{101}$$

$$= \sum_{i=1}^{N} \left[\int_{x_{i-1}}^{x_i} f(x)dx - h[f(x_{i-1} + f(x_i)]/2 \right]. \tag{102}$$

Then, by applying the theorem to each step in the summation, this yields

$$|\mathcal{E}| \leq \frac{h^3}{12} \sum_{i=1}^{N} \left[\max_{\zeta \in [x_{i-1}, x_i]} |f''(\zeta)| \right] \tag{103}$$

$$\leq \frac{(b-a)^3}{12N^2} M_2. \tag{104}$$